Electronic ISSN: 1309-0267

International Journal of Engineering & Applied Sciences

IJEAS

I J E A S

Volume 11, Issue 3
2019

Published by Akdeniz University

Editorial Board

(The name listed below is not Alphabetical or any title scale)

Abstracting & Indexing

IJEAS provides unique **DOI** link to every paper published.

Editorial Scope

The journal presents its readers with broad coverage across some branches of engineering and science of the latest development and application of new solution algorithms, artificial intelligent techniques innovative numerical methods and/or solution techniques directed at the utilization of computational methods in solid and nano-scaled mechanics.

International Journal of Engineering & Applied Sciences (IJEAS) is an Open Access Journal

International Journal of Engineering & Applied Sciences (IJEAS) publish original contributions on the following topics:

Numerical Methods in Solid Mechanics

Nanomechanic and applications

Microelectromechanical systems (MEMS)

Vibration Problems in Engineering

Higher order elasticity (Strain gradient, couple stress, surface elasticity, nonlocal elasticity) Applied Mathematics

CONTENTS

International Journal of Engineering & Applied Sciences (IJEAS)
Vol.11, Issue 3 (2019) 414-427
http://dx.doi.org/10.24107/ijeas.567374
Int J Eng Appl Sci 11(3) (2019) 414-427

Fitted Operator Average Finite Difference Method for Solving Singularly Perturbed Parabolic Convection- Diffusion Problems

Tesfaye Aga [a], Gemechis File [b], Guy Degla [c]*

[a,b]Department of Mathematics, Jimma University, Jimma, P. O. Box 378, Ethiopia
[c]Institut de Mathematiques et de Sciences Physiques (IMSP),UAC, Benin

E-mail address: tesfayeaga2@gmail.com[a*], gammeef@gmail.com[b], gdegla@gmail.com[c]

ORCID numbers of authors:
0000-0001-6766-4803[a], 0000-0003-1889-4690[b], 0000-0003-1162-6140[c]

Received date: 18.05.2019
Accepted date: 25.07.2019

Abstract

In this paper, we study a fitted operator average finite difference method for solving singularly perturbed parabolic convection-diffusion problems with boundary layer at right side. After discretizing the solution domain uniformly, the differential equation is replaced by average finite difference approximation which gives system of algebraic equation at each time levels. The stability and consistency of the method established very well to guarantee the convergence of the method. Furthermore, some numerical results are given to support our theoretical results and to validate the betterment of using fitted operator methods.

Keywords: Fitted operator, singular perturbation, parabolic problems, finite difference.

1. Introduction

The one dimensional partial differential equation:

$$\frac{\partial u}{\partial t}(x,t) = \alpha^2 \frac{\partial^2 u}{\partial x^2}(x,t) + \frac{\partial u}{\partial x}(x,t) + u(x,t) + f(x,t) \tag{1}$$

is a parabolic equation that used to model different physical phenomena such as heat distribution in a rod, in which case $u(x,t)$ represents the temperature at a point x and time t and $\alpha^2 > 0$ is the terminal diffusivity of the material with its value depends on what material the rod is composed of. The differential equation of the form of Eq. (1) is also called heat or diffusion equation. We assume that the left end at $x = 0$ a prescribed temperature $u_0(t)$ and the right end at $x = 1$ a prescribed temperature $u_1(t)$, which produces the boundary conditions $u(0,t) = u_0(t)$ and

$u(L,t) = u_1(t), \quad t > 0$. We also need information about the starting temperature that gives the initial condition, $u(x,0) = s(x), \ 0 < x < L.$

From the nature of modeling heat flow or chemical diffusion, the constant $\alpha^2 = \frac{K}{\delta\rho}$, where K is the termal conductivity, δ is specific heat and ρ is density of the material of the body. Here, assume that $K < \delta\rho$ so that let denote $\alpha^2 = \varepsilon$, ε is a parameter satisfying $0 < \varepsilon << 1$, then parabolic partial differential equation of Eq. (1) on the rectangle $Q := (0,1)\times(0,T]$ in the space time domain, where T is some fixed positive time with the stated condition called as the singularly perturbed convection – diffusion parabolic initial – boundary value problem of the form:

$$\frac{\partial u}{\partial t}(x,t) - \varepsilon\frac{\partial^2 u}{\partial x^2}(x,t) + a(x,t)\frac{\partial u}{\partial x}(x,t) + b(x,t)u(x,t) = f(x,t), \quad (x,t) \in Q \tag{2}$$

subject to the conditions:

$$\begin{aligned} u(x,0) &= s(x) \quad \text{on} \quad S_x := \{(x,0) : 0 \le x \le 1\} \\ u(0,t) &= q_0(t) \quad \text{on} \quad S_0 := \{(0,t) : 0 < t \le T\} \\ u(1,t) &= q_1(t), \quad \text{on} \quad S_1 := \{(1,t) : 0 < t \le T\} \end{aligned} \tag{3}$$

For convince the coefficients $a(x,t)$ and $b(x,t)$ are assumed to be sufficiently smooth functions such that:

$$a(x,t) \ge \beta_0 > 0 \quad \text{and} \quad b(x,t) \ge \beta_1 \ge 0 \tag{4}$$

Under sufficient smoothness and compatibility conditions imposed on the functions $s(x)$, $q_0(t)$, $q_1(t)$ and $f(x,t)$, the initial-boundary value problem admits a unique solution $u(x,t)$ the assumed condition $a(x,t) > 0$ which exhibits a boundary layer of width $O(\varepsilon)$ near the boundary $x = 1$ of Q , [7].

The singularly perturbed parabolic initial-boundary value problem of Eq. (2) is called convection-diffusion type with $\frac{\partial u}{\partial t}(x,t) + a(x,t)\frac{\partial u}{\partial x}(x,t)$ is considered as a convection term, but if $a(x,t) = 0$, then it is called as reaction–diffusion type whose reaction term $\frac{\partial u}{\partial t}(x,t) + b(x,t)u(x,t)$ with $-\varepsilon\frac{\partial^2 u}{\partial x^2}$ is the diffusion term in both cases.

In the past few decades, various ε-uniform numerical schemes are proposed in the literature for singular perturbation problems (SPPs). The numerical methods for SPPs are widely classified into two categories, namely, the fitted operator methods and the fitted mesh methods. In fitted operator methods, exponential fitting factors (artificial viscosity) will be used to control the rapid growth or decay of the numerical solution in the boundary layers [1]. Whereas, fitted mesh methods use nonuniform meshes, which will be fine or dense in the boundary layer regions and coarse outside

the layer regions. The well-known layer resolving fitted meshes are Bakhvalov meshes, which will be obtained from some nonlinear mesh generating function, and Shishkin meshes, which are piecewise-uniform and easy to obtain (see. [3], [4], [5] and [7]).

Different methods had been constructed to find the numerical solution of singularly perturbed parabolic problems; For instance, Spline in compression method [6], Bessel collocation method [8], A robust finite difference method [2]; A novel adaptive mesh strategy [9], An adaptive grid method [10] and so on. Hence, several numerical methods have been developed by different scholars for solving these problems and due to the importance of the problems in real life situations, the need to find numerical method(s) for approximating its solution is gainful. Thus, it is necessary to develop more accurate, stable and convergent numerical method for solving the singularly perturbed parabolic partial differential equations.

Therefore, the main objective of this study is to develop more accurate, stable and convergent a fitted operator average finite difference method for solving singularly perturbed parabolic convection- diffusion problems with right boundary layer at right side.

2. Formulation of the Method

Now, consider Eq. (2) on a particular domain $(x,t) \in Q := (0,1)\times(0,1]$ with the initial and boundary conditions in Eq. (3) and with remembering the condition in Eq. (4) to sure that the problem has boundary layer at $x = 1$. To solve this problem by the finite difference method, let M and N be positive integers. When working on $\bar{Q}$, we use a rectangular grid Q_h^k whose nodes are (x_m, t_n) for $m = 0,1,\ldots M$ and $n = 0,1,\ldots N$. Here, $0 = x_0 < x_1 < \ldots < x_M = 1$ and $0 = t_0 < t_1 < \ldots < t_N = T$ such grids are called tensor-product grids. For simplicity, throughout this material equidistant grids are considered as:

$$\begin{aligned} t_n &= nk, \quad k = \frac{T}{N}, \quad n = 0,1,2,\ldots, N \\ x_m &= mh, \quad h = \frac{1}{M}, \quad 1 = 0,1,2,\ldots, M \end{aligned} \tag{5}$$

Denote the approximate solution $u_m^n \approx u(x_m, t_n)$ at an arbitrary point (x_m, t_n). To obtain a finite difference scheme, we need to approximate the derivatives in Eq. (2) by some finite differences. Assume that the equation given in the form of Eq. (2) is satisfied at the point $\left(m,\, n+\frac{1}{2}\right)^{th}$ level. Then at this point Eq. (2) can be written as:

$$\frac{\partial u_m^{n+\frac{1}{2}}}{\partial t} - \varepsilon \frac{\partial^2 u_m^{n+\frac{1}{2}}}{\partial x^2} + a_m^{n+\frac{1}{2}} \frac{\partial u_m^{n+\frac{1}{2}}}{\partial x} + b_m^{n+\frac{1}{2}} u_m^{n+\frac{1}{2}} = f_m^{n+\frac{1}{2}} \tag{6}$$

For the derivatives with respect to *t*, using Taylor series expansion at the point $\left(m,\, n+\frac{1}{2}\right)$ we have:

$$u_m^{n+1} = u_m^{n+\frac{1}{2}} + \frac{k}{2}\frac{\partial u_m^{n+\frac{1}{2}}}{\partial t} + \frac{k^2}{8}\frac{\partial^2 u_m^{n+\frac{1}{2}}}{\partial t^2} + \frac{k^3}{48}\frac{\partial^3 u_m^{n+\frac{1}{2}}}{\partial t^3} + O(k^4) \tag{7}$$

$$u_m^{n} = u_m^{n+\frac{1}{2}} - \frac{k}{2}\frac{\partial u_m^{n+\frac{1}{2}}}{\partial t} + \frac{k^2}{8}\frac{\partial^2 u_m^{n+\frac{1}{2}}}{\partial t^2} - \frac{k^3}{48}\frac{\partial^3 u_m^{n+\frac{1}{2}}}{\partial t^3} + O(k^4) \tag{8}$$

Subtracting Eq. (8) from Eq. (7), gives the central difference approximation in such a point as

$$\frac{\partial u_m^{n+\frac{1}{2}}}{\partial t} = \frac{u_m^{n+1} - u_m^{n}}{k} + \tau_1 \tag{9}$$

where the truncation term $\tau_1 = -\frac{k^2}{24}\frac{\partial^3 u_m^{n+\frac{1}{2}}}{\partial t^3}$.

If we consider the other terms of Eq. (6) related to the points $(m,\, n)$ and $(m,\, n+1)$, using its average, which can be written:

$$-\varepsilon\frac{\partial^2 u_m^{n+\frac{1}{2}}}{\partial x^2} + a_m^{n+\frac{1}{2}}\frac{\partial u_m^{n+\frac{1}{2}}}{\partial x} + b_m^{n+\frac{1}{2}}u_m^{n+\frac{1}{2}} - f_m^{n+\frac{1}{2}} = \frac{L_x^N u_m^{n+1} + L_x^N u_m^{n}}{2} \tag{10}$$

where, $L_x^N u_m^{n+1} + L_x^N u_m^{n} = -\varepsilon\frac{u_{m+1}^{n+1} - 2u_m^{n+1} + u_{m-1}^{n+1}}{h^2} + a_m^{n+1}\frac{u_{m+1}^{n+1} - u_{m-1}^{n+1}}{2h} + b_m^{n+1}u_m^{n+1} - f_m^{n+1} +$

$$-\varepsilon\frac{u_{m+1}^{n} - 2u_m^{n} + u_{m-1}^{n}}{h^2} + a_m^{n}\frac{u_{m+1}^{n} - u_{m-1}^{n}}{2h} + b_m^{n}u_m^{n} - f_m^{n} + \tau_2$$

$$\tau_2 = h^2\left(\frac{\varepsilon}{12}\frac{\partial^4 u_m^{n+1}}{\partial x^4} - \frac{a_m^{n+1}}{6}\frac{\partial^4 u_m^{n+1}}{\partial x^4} + \frac{\varepsilon}{12}\frac{\partial^3 u_m^{n}}{\partial x^3} - \frac{a_m^{n}}{6}\frac{\partial^4 u_m^{n}}{\partial x^4}\right).$$

Substituting Eqs (9) and (10) into Eq. (6) gives:

$$\begin{aligned} &2u_m^{n+1} - 2u_m^{n} + k\left(-\varepsilon\frac{u_{m+1}^{n+1} - 2u_m^{n+1} + u_{m-1}^{n+1}}{h^2} + a_m^{n+1}\frac{u_{m+1}^{n+1} - u_{m-1}^{n+1}}{2h} + b_m^{n+1}u_m^{n+1}\right) \\ &+ k\left(-\varepsilon\frac{u_{m+1}^{n} - 2u_m^{n} + u_{m-1}^{n}}{h^2} + a_m^{n}\frac{u_{m+1}^{n} - u_{m-1}^{n}}{2h} + b_m^{n}u_m^{n}\right) = k\left(f_m^{n+1} + f_m^{n}\right) + \tau_3 \end{aligned} \tag{11}$$

where $\tau_3 = 2(\tau_1 + \tau_2)$.

To obtain the more accurate numerical solution and uniformly convergent numerical method, let introduce the fitting factors σ_1 and σ_2 on the obtained scheme Eq. (11) at both $(m,n)^{th}$ and $(m,n+1)^{th}$ level respectively as:

$$\begin{aligned} &2u_m^{n+1} - 2u_m^n + k\left(-\varepsilon\sigma_1 \frac{u_{m+1}^{n+1} - 2u_m^{n+1} + u_{m-1}^{n+1}}{h^2} + a_m^{n+1} \frac{u_{m+1}^{n+1} - u_{m-1}^{n+1}}{2h} + b_m^{n+1} u_m^{n+1} \right) \\ &+ k\left(-\varepsilon\sigma_2 \frac{u_{m+1}^{n} - 2u_m^{n} + u_{m-1}^{n}}{h^2} + a_m^{n} \frac{u_{m+1}^{n} - u_{m-1}^{n}}{2h} + b_m^{n} u_m^{n} \right) = k\left(f_m^{n+1} + f_m^{n} \right) \end{aligned} \tag{12}$$

To get the value of fitting factors σ_1 and σ_2, let denote $\rho = \frac{h}{\varepsilon}$ and after multiplying both side by h then evaluate the limit both sides of Eq.(12) as $h \to 0$ gives:

$$\begin{aligned} &\lim_{h\to 0}\left(-\frac{\sigma_1}{\rho}(u_{m+1}^{n+1} - 2u_m^{n+1} + u_{m-1}^{n+1}) + \frac{a_m^{n+1}}{2}(u_{m+1}^{n+1} - u_{m-1}^{n+1}) \right) + \\ &\lim_{h\to 0}\left(-\frac{\sigma_2}{\rho}(u_{m+1}^{n} - 2u_m^{n} + u_{m-1}^{n}) + \frac{a_m^{n}}{2}(u_{m+1}^{n} - u_{m-1}^{n}) \right) = 0 \end{aligned} \tag{13}$$

Since, the finite difference approximation terms are at $(m,n)^{th}$ and $(m,n+1)^{th}$ levels in different time direction, so that Eq. (13) satisfied if and only if:

$$\begin{cases} \lim_{h\to 0}\left(-\frac{\sigma_1}{\rho}(u_{m+1}^{n+1} - 2u_m^{n+1} + u_{m-1}^{n+1}) + \frac{a_m^{n+1}}{2}(u_{m+1}^{n+1} - u_{m-1}^{n+1}) \right) = 0 \\ \lim_{h\to 0}\left(-\frac{\sigma_2}{\rho}(u_{m+1}^{n} - 2u_m^{n} + u_{m-1}^{n}) + \frac{a_m^{n}}{2}(u_{m+1}^{n} - u_{m-1}^{n}) \right) = 0 \end{cases}$$

which is written as

$$\frac{2\sigma_1}{\rho} = \frac{\lim_{h\to 0} a_m^{n+1}\left(u_{m+1}^{n+1} - u_{m-1}^{n+1}\right)}{\lim_{h\to 0}\left(u_{m+1}^{n+1} - 2u_m^{n+1} + u_{m-1}^{n+1}\right)} \quad \text{and} \quad \frac{2\sigma_2}{\rho} = \frac{\lim_{h\to 0} a_m^{n}\left(u_{m+1}^{n} - u_{m-1}^{n}\right)}{\lim_{h\to 0}\left(u_{m+1}^{n} - 2u_m^{n} + u_{m-1}^{n}\right)} \tag{14}$$

Here, the main aim is to determine the values of the introduced fitted parameters σ_1 and σ_2; and as Roos *et. al*., [7] provide with the detailed proves for the asymptotic expansion of Eq. (2) with the conditions given in Eqs. (3) and (4) given by:

$$u(x,t) = u_0(x,t) + Ae^{-a(1,t)\frac{(1-x)}{\varepsilon}}$$

for the solution of its reduced form is $u_0(x,t)$ and A will be defined using the given boundary conditions that is written at the point $t = t_n$ as:

$$u^n(x) = u_0^n(x) + Ae^{-a^n(1)\frac{(1-x)}{\varepsilon}}$$

$$\lim_{h\to 0} u_m^n = u_0^n(0) + Ae^{-\frac{a_{(1)}^n}{\varepsilon}} e^{a_{(1)}^n m\rho} \tag{15}$$

From Eq. (11) inducing the indices, we get:

$$\lim_{h\to 0}\left(u_{m+1}^n - u_{m-1}^n\right) = Ae^{-\frac{a_{(1)}^n}{\varepsilon}} e^{a_{(1)}^n m\rho}\left(e^{a_{(1)}^n \rho} - e^{-a_{(1)}^n \rho}\right) \tag{16}$$

$$\lim_{h\to 0}\left(u_{m+1}^n - 2u_m^n + u_{m-1}^n\right) = Ae^{-\frac{a_{(1)}^n}{\varepsilon}} e^{a_{(1)}^n m\rho}\left(e^{a_{(1)}^n \rho} - 2 + e^{-a_{(1)}^n \rho}\right) \tag{17}$$

Using Eqs. (15), (16) and (17), Eq. (14) becomes:

$$\sigma_1 = \frac{\rho a_{(1)}^{n+1}}{2}\coth\left(\frac{\rho a_{(1)}^{n+1}}{2}\right) \quad \text{and} \quad \sigma_1 = \frac{\rho a_{(1)}^{n}}{2}\coth\left(\frac{\rho a_{(1)}^{n}}{2}\right) \tag{18}$$

From Eq. (12) and the values in Eq. (18), the fitted operator finite difference scheme given by:

$$2u_m^{n+1} + k\left(-\varepsilon\sigma_1 \frac{u_{m+1}^{n+1} - 2u_m^{n+1} + u_{m-1}^{n+1}}{h^2} + a_m^{n+1}\frac{u_{m+1}^{n+1} - u_{m-1}^{n+1}}{2h} + b_m^{n+1}u_m^{n+1}\right) = 2u_m^n$$
$$-k\left(-\varepsilon\sigma_2 \frac{u_{m+1}^{n} - 2u_m^{n} + u_{m-1}^{n}}{h^2} + a_m^{n}\frac{u_{m+1}^{n} - u_{m-1}^{n}}{2h} + b_m^{n}u_m^{n}\right) + k\left(f_m^{n+1} + f_m^n\right)$$

This can be written as the recurrence relation of the form:

$$-E_m^{n+1}u_{m-1}^{n+1} + F_m^{n+1}u_m^{n+1} - G_m^{n+1}u_{m+1}^{n+1} = H_m^{n+1} \tag{19}$$

for $m = 1, 2, \ldots, M$ and $n = 0, 1, 2, \ldots, N$,

where $E_m^{n+1} = k\left(\frac{\varepsilon\sigma_1}{h^2} + \frac{a_m^{n+1}}{2h}\right)$, $F_m^{n+1} = 2 + k\left(\frac{2\varepsilon\sigma_1}{h^2} + b_m^{n+1}\right)$, $G_m^{n+1} = k\left(\frac{\varepsilon\sigma_1}{h^2} - \frac{a_m^{n+1}}{2h}\right)$

$$H_m^{n+1} = k\left(\frac{\varepsilon\sigma_2}{h^2} + \frac{a_m^n}{2h}\right)u_{m-1}^n + \left(2 - k\left(\frac{2\varepsilon\sigma_2}{h^2} + b_m^n\right)\right)u_m^n + k\left(\frac{\varepsilon\sigma_2}{h^2} - \frac{a_m^n}{2h}\right)u_{m+1}^n + k\left(f_m^{n+1} + f_m^n\right)$$

The system of equations to be solved is tridiagonal: equation number m in the system only involves unknowns with numbers $m-1$, m and $m+1$, so that the matrix of the system has non-zero elements

only on the diagonal and in the positions immediately to the left and to the right of the diagonal. The coefficients E_m^{n+1}, F_m^{n+1}, G_m^{n+1} and the right-hand side H_m^{n+1} are given, and we assume that they satisfy the conditions:-

$\left|E_m^{n+1}\right| > 0,\ \left|F_m^{n+1}\right| > 0,\ \left|G_m^{n+1}\right| > 0$ and $\left|F_m^{n+1}\right| > \left|E_m^{n+1}\right| + \left|G_m^{n+1}\right|$

These conditions ensure that the matrix is *diagonally dominant*, with the diagonal element in each row being at least as large as the sum of the absolute values of the other elements.

$$2 + k\left(\frac{2\varepsilon\sigma_1}{h^2} + b_m^{n+1}\right) \geq k\left(\frac{\varepsilon\sigma_1}{h^2} + \frac{a_m^{n+1}}{2h}\right) + k\left(\frac{\varepsilon\sigma_1}{h^2} - \frac{a_m^{n+1}}{2h}\right)$$

Therefore, $\left|F_i^{j+1}\right| > \left|E_i^{j+1}\right| + \left|G_i^{j+1}\right|$, It is easy to see that these conditions are satisfied by our difference equation system. Thus, Eq. (19) can be solved by Thomas algorithm.

3. Stability of the Method

A partial differential equation is well-posed if the solution of the partial differential equation is exists, and depends continuously on the initial condition and boundary conditions. The Von Neumann stability technique is applied to investigate the stability of the developed scheme in Eq. (15), by assuming that the solution of Eq. (15) at the grid point (x_m, t_n) is given by:

$$u_m^n = \xi^n e^{im\theta} \tag{20}$$

where $i = \sqrt{-1}$, θ is the real number and ξ is the amplitude factor.

Now, putting Eq. (20) into the homogeneous part of Eq. (19) gives:

$$\xi\left(-E_m^{n+1}e^{-i\theta} + F_m^{n+1} - G_m^{n+1}e^{i\theta}\right) = k\left(\frac{\varepsilon\sigma_2}{h^2} + \frac{a_m^n}{2h}\right)e^{-i\theta} + \left(2 - k\left(\frac{2\varepsilon\sigma_2}{h^2} + b_m^n\right)\right) + k\left(\frac{\varepsilon\sigma_2}{h^2} - \frac{a_m^n}{2h}\right)e^{i\theta}$$

$$\xi = \frac{2 - k\left(\frac{2\varepsilon\sigma_2}{h^2} + b_m^n\right) + k\frac{\varepsilon\sigma_2}{h^2}e^{-i\theta} + k\frac{a_m^n}{2h}e^{-i\theta} + k\frac{\varepsilon\sigma_2}{h^2}e^{i\theta} - k\frac{a_m^n}{2h}e^{i\theta}}{-E_m^{n+1}e^{-i\theta} + F_m^{n+1} - G_m^{n+1}e^{i\theta}}$$

But, $e^{\pm i\theta} = \cos\theta \pm i\sin\theta \quad \Rightarrow \begin{cases} e^{i\theta} + e^{-i\theta} = \cos\theta + i\sin\theta + \cos\theta - i\sin\theta = 2\cos\theta \\ e^{-i\theta} - e^{i\theta} = \cos\theta - i\sin\theta - (\cos\theta + i\sin\theta) = -2i\sin\theta \end{cases}$

and, we have the values of E_m^{n+1}, F_m^{n+1} and G_m^{n+1} from Eq. (15) which implies:

$$\xi = \frac{2 - 4k\dfrac{\varepsilon\sigma_2}{h^2}}{2 + 4k\dfrac{\varepsilon\sigma_1}{h^2}} - i\frac{k\dfrac{a_m^n}{h}\sin\theta}{2 + 4k\dfrac{\varepsilon\sigma_1}{h^2}}$$

The condition of stability is $\xi \le 1$ and for sufficiently small k, we have $\xi = 1$. Hence, the scheme given in Eq. (19) is stable for any value of mesh sizes in both with respect to x and t. Thus, the scheme in Eq. (19) is unconditionally stable.

4. Consistency of the method

Local truncation errors refer to the differences between the original differential equation and its finite difference approximations at grid points. To investigate the consistency of the method, we have the local truncation errors from Eqs (9), (10) and (11) given as:-

$$T_m^{n+1} = \tau_3 = 2\left(\tau_1 + \tau_2\right) \tag{21}$$

where $\tau_1 = -\dfrac{k^2}{24}\dfrac{\partial^3 u_m^{n+\frac{1}{2}}}{\partial t^3}$ and $\tau_2 = h^2\left(\dfrac{\varepsilon}{12}\dfrac{\partial^4 u_m^{n+1}}{\partial x^4} - \dfrac{a_m^{n+1}}{6}\dfrac{\partial^4 u_m^{n+1}}{\partial x^4} + \dfrac{\varepsilon}{12}\dfrac{\partial^3 u_m^n}{\partial x^3} - \dfrac{a_m^n}{6}\dfrac{\partial^4 u_m^n}{\partial x^4}\right)$.

Thus, the right hand side hand of Eq. (21) vanishes as $k \to 0$ and $h \to 0$ implies $T_m^{n+1} \to 0$.

Hence, the scheme is consistent with the order of convergence $O\left(k^2 + h^2\right)$. Therefore, the scheme developed in Eq. (19), is convergent. A consistent and stable finite difference method is **convergent** by Lax's equivalence theorem [7].

5. Numerical Examples and Results

To validate the applicability of the method, model problems have been considered and these examples have been chosen since they have been widely discussed in the literature.

Example 1: Consider the singularly perturbed parabolic problem:

$$\frac{\partial u}{\partial t} - \varepsilon\frac{\partial^2 u}{\partial x^2} + (1 + x(1-x))\frac{\partial u}{\partial x} = f(x,t), \quad (x,t) \in (0,1)\times(0,1]$$

subject to the conditions:

$$u(x,0) = s(x), \ 0 < x < 1$$
$$u(0,t) = 0 = u(1,t), \quad 0 \le t \le 1$$

We choose the initial data $s(x)$ and the source function $f(x,t)$ to fit with the exact solution:

$$u(x,t) = e^{-t}(e^{-\frac{1}{\varepsilon}} + x(1-e^{-\frac{1}{\varepsilon}}) - e^{-\frac{1-x}{\varepsilon}})$$

As the exact solution for this example is known, for each perturbation parameter ε, we calculate absolute maximum errors defined by:

$$E^{M,N} = \max_{(x_m,t_n)\in Q_\varepsilon^{M,N}} \left|u(x_m,t_n) - u_m^n\right|$$

where $u(x_m,t_n)$ and u_m^n respectively, denote the exact and approximate solution. In addition, we determine the corresponding order of convergence by:

$$R_\varepsilon^{M,N} = \frac{\log(E_\varepsilon^{M,N}) - \log(E_\varepsilon^{2M,2N})}{\log(2)}$$

Table 1. Comparison of maximum absolute errors for Example 1 at the number of intervals *M*, *N*

$\varepsilon\downarrow$	32, 10	64, 20	128, 40	256, 80	512, 160
With fitting factors					
10^0	3.2004e-06	7.8950e-07	1.9651e-07	4.9075e-08	1.2263e-08
10^{-1}	3.6140e-04	8.9287e-05	2.2181e-05	5.5427e-06	1.3851e-06
10^{-2}	1.2823e-02	2.9914e-03	5.4598e-04	1.2963e-04	3.2304e-05
10^{-3}	1.7476e-02	9.1719e-03	4.6673e-03	2.0168e-03	5.3827e-04
10^{-4}	1.7476e-02	9.1720e-03	4.6963e-03	2.3759e-03	1.1949e-03
Without fitting factors					
10^0	1.8093e-06	4.4513e-07	1.1081e-07	2.7681e-08	6.9183e-09
10^{-1}	2.3684e-03	5.8236e-04	1.4515e-04	3.6249e-05	9.0592e-06
10^{-2}	3.0639e-01	9.9446e-02	2.0645e-02	4.3908e-03	1.0958e-03
10^{-3}	9.5155e-01	8.5929e-01	6.7603e-01	4.0072e-01	1.5072e-01
10^{-4}	1.1607e+00	1.1820e+00	1.1463e+00	1.0424e+00	9.2024e-01

Table 2. Comparison of maximum absolute errors for Example 1 at the number of intervals *M*, *N*

$\varepsilon\downarrow$	32, 10	64, 20	128, 40	256, 80	512, 160
Present method					
10^0	3.2004e-06	7.8950e-07	1.9651e-07	4.9075e-08	1.2263e-08
10^{-2}	1.2823e-02	2.9914e-03	5.4598e-04	1.2963e-04	3.2304e-05
10^{-4}	1.7476e-02	9.1720e-03	4.6963e-03	2.3759e-03	1.1949e-03
Results in [1]					
10^0	6.8921e-04	3.7085e-04	1.9290e-04	9.8440e-05	4.9739e-05
10^{-2}	7.1532e-02	4.5000e-02	2.6393e-02	1.4579e-02	7.1423e-03
10^{-4}	9.3382e-02	5.5430e-02	3.9185e-02	2.1997e-02	1.1787e-02

Table 3. Comparison of Rate of convergence for Example 1 at the number of intervals *M, N*

$\varepsilon\downarrow$	32, 10	64, 20	128, 40	256, 80
Present method				
10^{0}	2.0192	2.0063	2.0015	2.0007
10^{-2}	2.0998	2.4539	2.0744	2.0046
10^{-4}	0.9301	0.9657	0.9831	0.9916
Results in [1]				
10^{0}	0.8941	0.9430	0.9705	0.9849
10^{-2}	0.7203	0.7853	0.8376	0.8912
10^{-4}	0.8211	0.9108	0.9624	0.9674

Example 2: Consider the singularly perturbed parabolic problem:

$$\frac{\partial u}{\partial t}-\varepsilon\frac{\partial^2 u}{\partial x^2}+(1+x^2+\frac{1}{2}\sin\pi x)\frac{\partial u}{\partial x}+(1+x^2+\frac{1}{2}\sin\frac{\pi t}{2})u(x,t)=f(x,t),$$

for $(x,t)\in(0,1)\times(0,1]$ and the source function $f(x,t)=x^3(1-x)^3t(1-t)\sin\pi t$

subject to the conditions:

$$u(x,0)=0,\ 0<x<1$$
$$u(0,t)=0=u(1,t),\quad 0\le t\le 1$$

Since the exact solution is not known, we use the double mesh principle to obtain the maximum absolute errors and to investigate the rate of convergence.

Table 4. Comparison of maximum absolute errors for Example 2 at the number of intervals *M, N*

$\varepsilon\downarrow$	32, 16	64, 32	128, 64	256, 128	512, 256
With fitting factors					
10^{0}	8.7112e-05	1.8949e-05	4.1396e-06	1.0346e-06	2.5881e-07
10^{-1}	3.4987e-04	8.7838e-05	2.1985e-05	5.4998e-06	1.3751e-06
10^{-2}	1.7357e-03	6.7495e-04	1.9879e-04	5.2071e-05	1.3176e-05
10^{-3}	1.8971e-03	1.0473e-03	5.5534e-04	2.7537e-04	1.0935e-04
10^{-4}	1.8971e-03	1.0473e-03	5.5579e-04	2.8673e-04	1.4569e-04
Without fitting factors					
10^{0}	8.7165e-05	1.8953e-05	4.1427e-06	1.0353e-06	2.5902e-07
10^{-1}	5.3647e-04	1.3050e-04	3.2470e-05	8.1069e-06	2.0261e-06
10^{-2}	3.8366e-02	1.6433e-02	4.9141e-03	1.0717e-03	2.5149e-04
10^{-3}	1.1881e-01	1.0523e-01	8.0985e-02	5.0465e-02	2.3456e-02
10^{-4}	1.3687e-01	1.3825e-01	1.3548e-01	1.2804e-01	1.1388e-01

Table 5. Comparison of Rate of convergence for Example 2 at the number of intervals *M*, *N*

$\varepsilon\downarrow$	32, 16	64, 32	128, 64	256, 128
With fitting factors				
10^{0}	2.2007	2.1946	2.0004	1.9991
10^{-1}	1.9939	1.9983	1.9991	1.9998
10^{-2}	1.3627	1.7635	1.9327	1.9826
10^{-3}	0.8571	0.9152	1.0120	1.3324
10^{-4}	0.8571	0.9141	0.9548	0.9768
Without fitting factors				
10^{0}	2.2013	2.1938	2.0005	1.9989
10^{-1}	2.0394	2.0069	2.0019	2.0004
10^{-2}	1.2232	1.7416	2.1970	2.0913
10^{-3}	0.1751	0.3778	0.6824	1.1053
10^{-4}	- 0.0145	0.0292	0.0815	0.1691

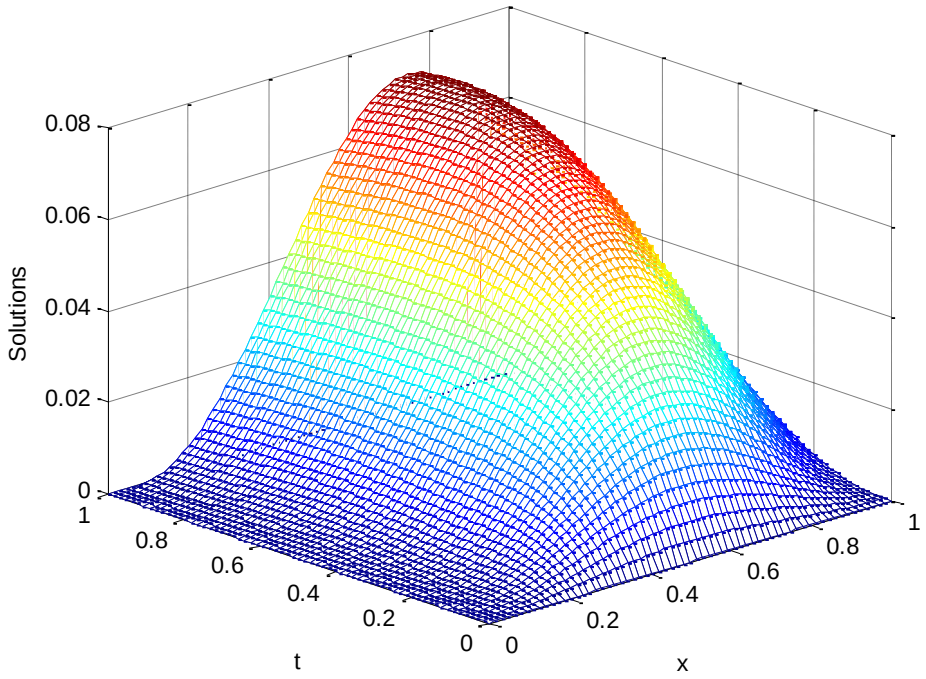

Fig. 1. Behavior of the solutions for Example 2 at $M = N = 64$ and $\varepsilon = 10^{-4}$

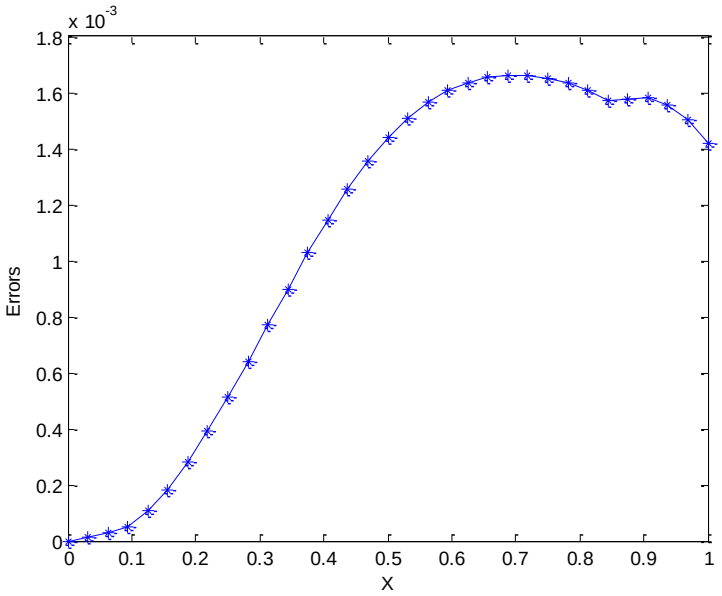

Fig. 2. Pointwise absolute errors for Example 2 at $M = N = 32$ and $\varepsilon = 10^{-2}$

6. Discussion

We have discussed a fitted operator average finite difference method for solving singularly perturbed parabolic convection- diffusion problems which have right boundary layer. The basic mathematical procedures are define the model problem, discretize the solution domain uniformly, replace the differential equation by central difference approximation to the time derivative and approximate the other terms by the average of the central approximation related to two level points. Then the central finite difference approximation gives three-term recurrence relations at each time level with respect to the spatial direction which is diagonal dominate, so that solved by Thomas algorism. Also, the stability and consistency of the method investigated very well to guarantee the convergence of the method.

It can be seen from the results obtained and presented in Tables (1) and (4) shows that, the numerical methods presented in this study converge in the maximum absolute errors with more accurate solution than without fitted numerical method. For each ε, M and N in Tables (1 - 5) shows the effectiveness of applying fitted operator in order to obtain more accurate numerical solution and to show the second order rate of convergence . Thus, from the results presented, we have evidence that the maximum absolute errors and the corresponding rate of convergence calculated using the present method is more accurate with higher rate of convergence than the existing methods. Figure 1, indicates the physical behavior of the problem while Figure 2 to indicates the position of boundary layer.

7. Conclusion

In this study, we have discussed a fitted operator average finite difference method for solving singularly perturbed parabolic convection- diffusion problems. In order to obtain more accurate numerical solution, introduce and determine the values of fitting parameter. As shown in the investigation of consistency, the present method is second order convergent with respect to the two independent variables. The stability and consistency have been established very well to guarantee the convergence of the method. Moreover, as some numerical results are calculated to support the theoretical results and to demonstrate the effectiveness and the advancement of using fitting operator method has a better numerical accuracy compared to without fitted operator and other methods.

Reference

[1] Gowrisankar S., Srinivasan N., Robust numerical scheme for singularly perturbed convection–diffusion parabolic initial–boundary-value problems on equidistributed grids, Computer Physics Communications, 185, 2008-2019, 2014

[2] Munyakazi J. B., A Robust Finite Difference Method for Two-Parameter Parabolic Convection-Diffusion Problems, *An International Journal of Applied Mathematics & Information Sciences*, Vol. 9(6), 2877-2883, 2015

[3] Miller H. J.J, O'Riordan E. and Shishkin I. G., Fitted numerical methods for singular perturbation problems, Error estimate in the maximum norm for linear problems in one and two dimensions, World Scientific, 1996

[4] Das P. and Mehrmann V., Numerical solution of singularly perturbed convection-diffusion-reaction problems with two small parameters, *BIT Numer Math* DOI 10.1007/s10543-015-0559-8, 2015

[5] Rai P. and. Sharma K. K., Singularly perturbed parabolic differential equations with turning point and retarded arguments, *IAENG International Journal of Applied Mathematics*, 45:4, IJAM_45_4_20, 2015

[6] Mohanty R. K., Dahiya V., Khosla N., Spline in Compression Methods for Singularly Perturbed 1D Parabolic Equations with Singular Coefficients, *Open Journal of Discrete Mathematics*, 2, 70-77, 2012

[7] Roos G. H., Stynes M.and Tobiska L., Robust numerical methods for singularly perturbed differential equations, Convection-diffusion-reaction and flow problems, Springer-Verlag Berlin Heidelberg, Second Edition, 2008

[8] Suayip Y. S. and Sahin N., Numerical solutions of singularly perturbed one-dimensional parabolic convection–diffusion problems by the Bessel collocation method, *Applied Mathematics and Computation* 220, 305–315, 2013

[9] Vivek K. and Srinivasan B., A novel adaptive mesh strategy for singularly perturbed parabolic convection diffusion problems, *Differ Equ Dyn Syst*, DOI 10.1007/s12591-017-0394-2, 2017
[10]. Yanping C. and Li-Bin L., An adaptive grid method for singularly perturbed time – dependent convection diffusion problems, *Commun. Comput. Phys*, 20, 1340-1358, 2016.

International Journal of Engineering & Applied Sciences (IJEAS)
Vol.11, Issue 3 (2019) 428-444
http://dx.doi.org/10.24107/ijeas.621160
Int J Eng Appl Sci 11(3) (2019) 428-444

Computational Techniques for The Evaluation of Inhomogeneity Parameters on Transient Conduction in Functionally Graded Layers

Mehmet N. Balci [*], *Barış Sabuncuoğlu*

Mechanical Engineering Department, Hacettepe University, 06800, Ankara, Turkey

[*]*E-mail address*: mehmetbalci@hacettepe.edu.tr , barissabuncuoglu@hacettepe.edu.tr

ORCID numbers of authors:
0000-0002-4416-6761[*], *0000-0001-5156-746X*

Received date: 17.09.2019
Accepted date: 01.11.2019

Abstract

Transient thermal response of a functionally graded material (FGM) layer is considered and individual effects of inhomogeneity parameters on temperature distribution are examined. Transient conduction equation has variable coefficients controlling conductivity, mass density and specific heat capacitance due to the material property variation along the thickness of the graded layer. In order to solve the time dependent conduction equation for the unknown interior temperatures, computational methods are employed based on finite difference and finite element methods. Governing partial differential equation is discretized in space and time grids and computer codes are developed to implement explicit and implicit schemes. Results of explicit and implicit schemes are compared with those found by finite element method. A very good agreement is achieved for the applied boundary and initial conditions. Parametric study reveals the individual influences of various inhomogeneity parameters of FGM upon time dependent temperature distribution of a functionally graded layer. The results of the direct comparison study indicate that inhomogeneity parameters for specific heat and mass density have greater influence on temperature distribution than that for thermal conductivity.

Keywords: Functionally Graded Layer, Transient Heat Conduction, Computational Methods, Material Inhomogeneity

1. Introduction

Functionally graded materials (FGMs) are advanced composites involving two or more constituent phases. These materials are regarded as advanced engineering composites designed to meet material demands with the variance of via the spatial gradation in the structure. Originally considered as thermal barrier coatings for aerospace structures and fusion reactors, FGMs were also used as structural components in transportation, energy, electronics and biomedical engineering for the general use in high temperature environment in the last decade [1]. Generally, there are three different methods to obtain compositional gradient in the material which includes gas based, liquid phase and solid phase methods. Hence, physically or chemically tailored properties are obtained in the structure. Chemical Vapor Deposition (CVD), Physical Vapor Deposition (PVD), ion plating, plasma spraying and ion mixing are some examples of gas-based methods to fabricate FGMs. Methods such as centrifugal casting, slip casting, chemical solution deposition (CSD), electrochemical

gradation are some liquid phase examples to product FGMs. Furthermore, spark plasma sintering and powder metallurgy techniques can be given for examples of solid phase methods [2]. Bellur-Ramaswamy et al. [3] developed an algorithm to optimize continuous quench process parameters to produce functionally graded aluminum alloy extrudes. The gradual changes in volume fraction of the constituents and non-homogenous structure provides continuous graded macroscopic properties, such as hardness, wear resistance, corrosion resistivity, thermal conductivity, specific heat and mass density that are critical for thermal barrier coatings (TBCs) as well as thermal protection of the re-entry capsule, furnace liners, body armour, piezoelectric actuators and electromagnetic sensors [4-7]. Therefore, there have been many studies related with the thermal properties of these materials and their interaction with their structural behavior. Numerical methods are frequently applied to investigate such properties to understand their thermal behavior in the design stage. It was reported that repeated hot gas flow tests indicated that utilization of FGM thermal barrier coatings (TBCs) enhanced the resistance to cracking and delamination at high temperatures when compared to conventional coatings. For example, ZrO_2/Ni functionally graded material (FGM) was used as TBC for the rocket engine and no delamination was observed after 550 seconds of combustion. ZrO_2 stabilized with Y_2O_3 functionally graded material (FGM) was used as TBC for turbine blades and it was seen that this material performed excellent resistance to erosion and thermal shock [8-9]. Reddy and Chin [10] investigated the dynamic thermoelastic response of functionally graded cylinders and plates, thermomechanical coupling was included and a finite element model was developed. Yang [11] proposed a research based on finite element analysis to examine the temperature distribution, thermal stresses and failure criteria of a multi-dimensional functionally graded material (FGM) plate which was composed of ZrO_2 and Ti-6Al-4V and Al_2O_3 under steady-state, heating and sudden cooling conditions. Analytical method was proposed to analyze the transient heat conduction analysis in a cylindrical shell made of functionally graded material where material properties vary with the power law through the thickness [12]. The response of a circular cylindrical thin shell made of the functionally graded material (FGM) based on the generalized theory of thermoelasticity was determined. Power law was adopted for the spatial variation of the thermoelastic properties [13]. Mechanical and thermal buckling of FGM conical shell panels made of Al/ZrO_2, SUS304/Si_3N_4 and Al_2O_3/Ti-6Al-4V were investigated through an element-free method by Zhao and Liew [14].

Sharma et al. [15] constructed a finite element model to investigate the steady state temperature field in FGM layer which was composed of Zirconia and Aluminum. Through the thickness temperature distribution and thermal stresses in a plate which was made of functionally graded material were determined by Cho and Oden [16] using Crank-Nicolson-Galerkin scheme. It was reported in the study conducted by Nemat-Alla [17] that two-dimensional graded materials (2D-FGMs) had a great potential for minimization of temperatures, thermal and residual stresses under a severe thermal loading cycle that includes of heating followed by cooling operations. Sladdek et al. [18] proposed an advanced computational method based on local boundary integral equations for transient heat conduction analysis in continuously non-homogenous functionally graded materials (FGMs). Sadowski and Nakonieczny [19] focused on numerical study based on researching the FGM grading pattern impact on the temperature distribution in the cylindrical plates made of Al_2O_3/ZrO_2 under the thermal shock condition. A meshfree, semi-discrete finite element method was proposed for the solution of the thermal shock problem for a thin, cylindrical plate made of FGM ceramics, and an explicit finite difference method was utilized for the temporal discretization [20]. A multiple reciprocity boundary face method was developed to investigate the transient heat conduction analysis of functionally graded materials [21]. Li and

Wen [22] put forward a finite block method based on the Lagrange series to solve transient heat conduction problem in a functionally graded media regarding one dimensional to three dimensional conduction cases. A thermal conduction analysis of layered functionally graded materials composed of Ni and Carbon nanotube was performed by Olatunji- Ojo et al. [23] using a finite element code and parametric studies were carried out using different cooling times, different mixing rules and different heat transfer coefficients. Jin [24] examined the transient heat conduction in a functionally graded plate subjected to gradual cooling and heating at its boundaries and asymptotic analysis and integration technique were used to obtain a closed form asymptotic solution of temperature field in FGM plate for short times. Determination of through the thickness temperature distribution in functionally graded materials (FGMs) has significant importance since it directly influences the failure mechanism.

In the present study, we develop computer codes based on explicit and implicit schemes to determine the transient temperature distribution in a layer made of FGM and compare results with those obtained through the finite element analysis. Then, the separate influences of inhomogeneity parameters for the thermal conductivity, thermal capacitance and the mass density on temperature distribution in a graded layer are determined. The main novelty of the present study is the investigation of the influences of these inhomogeneity constants separately on the temperature distribution in FGM layers, individually and determination of the dominance of each parameter. Governing partial differential equation has variable coefficients of each material property and solution is performed keeping the generality. It is demonstrated that computational methods based on explicit and implicit schemes can efficiently be applied to such conduction problems including non-homogenous materials and they are able to provide fast and accurate solutions. In addition to that, although there have been many works in the literature which utilized some kind of different computational methods to examine the transient heat conduction problem in FGM layers, none of them compared the results of developed computational techniques with each other. Thus, another novelty of the paper is providing the comparison of the temperature results for an FGM layer obtained by explicit, implicit and FEA methods. It is believed that results of this study will be helpful for material designers to understand the transient thermal response of graded layers designated especially for thermal barrier coatings in harsh environments.

2. FGM Material and Properties

The functionally graded material (FGM) considered made of ceramic and metal phases is illustrated in Fig.1. One side of functionally graded layer is composed of 100% ceramic phase whereas the other side of the layer is composed of 100% metallic phase with the intermediate transition region in between. Material properties are denoted by exponential functions varying in x-axis. A schematic illustration of a continuously graded microstructure in FGM is provided by Chan et al. [25]. As provided in [26-27], thermal conductivity, heat capacitance and density of the functionally graded layer are defined by the exponential functions:

$$k = k_0 \exp(\gamma_1 x), \tag{1}$$

$$c = c_0 \exp(\gamma_2 x), \tag{2}$$

$$\rho = \rho_0 \exp(\gamma_3 x). \tag{3}$$

where k_0, c_0 and ρ_0 are the thermal conductivity, heat capacitance and mass density at the metallic (left) surface $(x=0)$. γ_1, γ_2 and γ_3 respectively show the inhomogeneity constants for thermal conductivity, specific heat capacitance and mass density and these constants are assumed to be different from each other in the present study. ZrO_2 and Ti-6Al-4V are referencing ceramic and metallic materials utilized in the present study and their thermal properties are provided in Table 1.

Table 1. Material properties of ZrO_2 and Ti-6Al-4V (Fujimoto and Noda [28]).

Material	**ZrO_2**	**Ti-6Al-4V**
Thermal conductivity (W/mK)	2.036	18.1
Heat capacitance (j/kgK)	615.6	808.3
Density (kg/m^3)	5600	4420

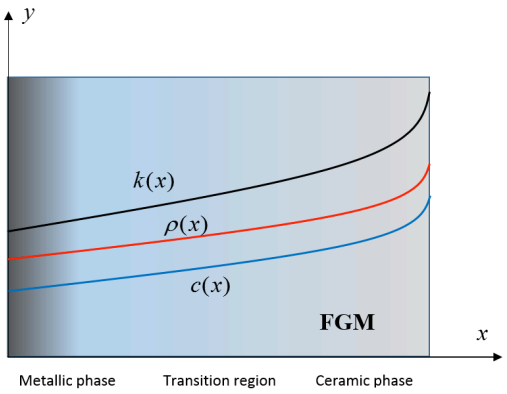

Fig. 1. The schematic illustration of functionally graded material possessing different inhomogeneity constants for thermal properties

3. Equation of Conduction and Boundary Conditions

In order to find the time dependent temperature distribution inside the FGM layer, the following heat conduction equation should be derived. One of the main contributions of this study over previous studies is to taking into consideration of spatial variation of each thermal properties separately, hence derived heat conduction equation is different that adopted in the previous studies. The derivation of conduction equation is shown in Eqs. (4)-(5) which involves variable parameters for thermal conductivity, heat capacitance and mass density.

$$\frac{\partial k(x)}{\partial x}\frac{\partial T}{\partial x}+k(x)\frac{\partial^2 T}{\partial x^2}=\rho(x)c(x)\frac{\partial T}{\partial t}. \tag{4}$$

$$\frac{\partial T}{\partial t}=\gamma_1\,\alpha(x)\frac{\partial T}{\partial x}+\alpha(x)\frac{\partial^2 T}{\partial x^2}. \tag{5}$$

The thermal diffusivity for the FGM layer is expressed to be:

$$\alpha(x) = \alpha_0 \exp(\gamma_1 - \gamma_2 - \gamma_3)x \tag{6}$$

$$\alpha_0 = \frac{k_0}{\rho_0 c_0}. \tag{7}$$

Two different boundary and initial condition cases are applied to the boundary value problem and these conditions are given in Table 2.

Table 2. Applied boundary and initial conditions

Case 1	**Case 2**
$T_1 = 0\,K,$	$T_1 = T_0\,K,$
$T_2 = 0\,K,$	$T_2 = 2T_0\,K,$
$T(x,0) = T_0 \times \sin(\pi x/L)\,K$	$T(x,0) = T_0\,K$

where $T_0 = 1000\,K$.

4. Computational Techniques Applied for the Transient Thermal Analysis of FGM

The addressed heat conduction equation is discretized utilizing the finite difference formula. Temperature at the left surface is denoted by $T_{0,0}$ and that at the right surface is shown by $T_{N,0}$. This discretization in space and time parameters is illustrated in Fig. 2. After discretization step is completed, formulations for explicit and implicit schemes are developed.

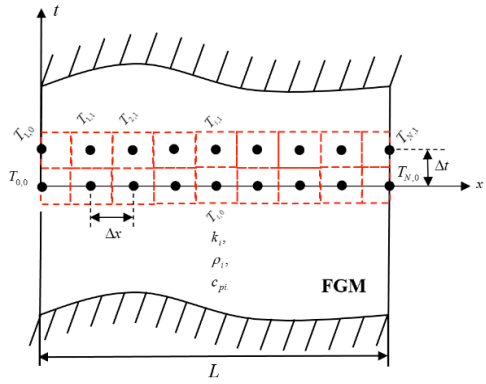

Fig. 2. Discretized numerical model prepared for the numerical analysis

In the following subsections 4.1 and 4.2, explicit and implicit formulations are provided. The derived formulations are implemented into MATLAB.

4.1. Explicit method formulation

The general explicit method finds the solution of node *i* at time *j+1* using the temperature information available at nodes *i-1*, *i* and *i+1* at time *j*. Temperature value of point *i* at time *j+1*, $T_{i,j+1}$ is calculated using the temperature values at time *j* using the temperature values of two neighboring points. We develop a formulation based on the explicit method to find the temperature distribution along the FGM layer whose thermal properties vary with the *x*-

coordinate. In order to discretize the time dependent heat conduction equation in space and time domains, the following central difference formulae are utilized.

$$\frac{\partial T}{\partial t} = \frac{T_{i,j+1} - T_{i,j}}{\Delta t} + O(\Delta t), \tag{8}$$

$$\frac{\partial T}{\partial x} = \frac{T_{i+1,j} - T_{i-1,j}}{2\Delta x} + O(\Delta x^2), \tag{9}$$

$$\frac{\partial^2 T}{\partial x^2} = \frac{T_{i-1,j} - 2T_{i,j} + T_{i+1,j}}{(\Delta x)^2} + O(\Delta x^2). \tag{10}$$

When Eqs. (8-10) are substituted into Eq. (5) and after performing necessary mathematical manipulations, temperature at space i and time $j+1$, $T_{i,j+1}$ is calculated through the following equation.

$$\begin{aligned} T_{i,j+1} = T_{i,j} + \frac{\gamma_1 \alpha_0}{2} \exp\{(\gamma_1 - \gamma_2 - \gamma_3)x_i\} \left(\frac{\Delta t}{\Delta x}\right) \left[T_{i+1,j} - T_{i-1,j}\right] + \\ + \alpha_0 \exp\{(\gamma_1 - \gamma_2 - \gamma_3)x_i\} \left(\frac{\Delta t}{\Delta x^2}\right) \left[T_{i-1,j} - 2T_{i,j} + T_{i+1,j}\right]. \end{aligned} \tag{11}$$

Since explicit scheme calculates temperature distribution at time $j+1$ using the temperature information at time j, it is open to any instability problems. Since material properties of FGM layer vary with respect to spatial coordinate, the dimensionless mesh Fourier number for this material is not constant, so we need to define mesh Fourier number for all the grid points as,

$$\tau_i = \frac{\alpha_i \Delta t}{(\Delta x)^2} \tag{12}$$

where

$$\alpha_i = \frac{k_i}{\rho_i c_{pi}} \tag{13}$$

In Eq. (13), the subscript i shows the properties of the FGM material at the spatial coordinate x_i. In order to obtain stable numerical solutions using explicit scheme, the following condition must be satisfied for all the grid points throughout the functionally graded layer. If this condition is not satisfied at least one of the grid points, the numerical solution of the overall system will not be stable and properly found.

$$\tau_i = \frac{\alpha_i \Delta t}{(\Delta x)^2} \le \frac{1}{2}. \tag{14}$$

4.2. Implicit method formulation

As an implicit method, the Crank-Nicolson (C-N) scheme is considered for the transient thermal analysis of FGM layer. The Crank-Nicolson (C-N) scheme finds the solution of nodes *i-1*, *i* and *i+1* at time *j+1* using the information available at nodes *i-1*, *i* and *i+1* at time *j*. In this method, temperature values of points *i-1*, *i* ,*i+1* at time *j+1* are calculated utilizing the temperature values of points *i-1, i, i+1* at time *j*. In this section, the formulation based on the implicit (C-N) method is provided for the thermal analysis of FGM layer. In order to discretize the time dependent heat conduction equation in space and time variables, the following central difference formulae are employed.

$$\frac{\partial T}{\partial t} = \frac{T_{i,j+1} - T_{i,j}}{\Delta t} + O(\Delta t), \tag{15}$$

$$\frac{\partial T}{\partial x} = \frac{T_{i+1,j} - T_{i-1,j}}{2\Delta x} + O(\Delta x^2), \tag{16}$$

$$\frac{\partial^2 T}{\partial x^2} = \frac{T_{i-1,j} - 2T_{i,j} + T_{i+1,j}}{(\Delta x)^2} + O(\Delta x^2). \tag{17}$$

Utilizing the finite difference formula, the heat conduction equation is discretized as follows:

$$\begin{aligned} \frac{T_{i,j+1} - T_{i,j}}{\Delta t} &= \gamma_1 \alpha_0 \exp\left(\left(\gamma_1 - \gamma_2 - \gamma_3\right) x_i\right)\left(\frac{T_{i+1,j} - T_{i,j}}{\Delta x}\right) + \\ &+ \frac{\alpha_0 \exp\left(\left(\gamma_1 - \gamma_2 - \gamma_3\right) x_i\right)}{2\left(\Delta x\right)^2}\left(\left(T_{i+1,j+1} - 2T_{i,j+1} + T_{i-1,j+1}\right) + \left(T_{i+1,j} - 2T_{i,j} + T_{i-1,j}\right)\right) \end{aligned} \tag{18}$$

Rearrangement of Eq. (18) produces the following equation:

$$-f_{i-1} T_{i-1,j+1} + g_i T_{i,j+1} - f_{i+1} T_{i+1,j+1} = f_{i-1} T_{i-1,j} + l_i T_{i,j} - s_{i+1} T_{i+1,j} \tag{19}$$

where coefficients depending on space variables can be denoted by,

$$f_i = \frac{\alpha_0}{2\left(\Delta x\right)^2} \exp\left(\left(\gamma_1 - \gamma_2 - \gamma_3\right) x_i\right), \tag{20}$$

$$d_i = \frac{\gamma_1}{\Delta x} \alpha_0 \exp\left(\left(\gamma_1 - \gamma_2 - \gamma_3\right) x_i\right), \tag{21}$$

$$g_i = \frac{1}{\Delta t} + 2f_i, \tag{22}$$

$$l_i = \frac{1}{\Delta t} - 2f_i - d_i, \tag{23}$$

$$s_i = d_i + f_i. \tag{24}$$

Since the layer is made of functionally graded material, parameters f_i, d_i, g_i, l_i and s_i are not constant parameters. Eq. (19) is expanded in space and time grids using index parameters $j=1,2,...,M$ and $i=1,2,...,N$ where M and N indicates the boundary points of time and space grids. Hence, T_{NM} shows the temperature of point N at time M. In our parametric analyses, the final time of simulation is specified as $t_f = 5s$ and 0.01s time intervals are used. The distance between two neighboring nodes is specified as $\Delta x = 0.0005m$. When Eq. (19) is expanded for $j=\{1,2,3,...,M\}$ and $i=\{2,3,4,...,N\}$, the equation set is obtained as follows:

$$\begin{bmatrix} g_2 & -f_3 & 0 & 0 & ... & 0 \\ -f_2 & g_3 & -f_4 & 0 & ... & 0 \\ 0 & -f_3 & g_4 & -f_5 & ... & 0 \\ 0 & 0 & -f_4 & g_5 & -f_6 & 0 \\ ... & ... & ... & -f_{N-3} & g_{N-2} & -f_{N-1} \\ 0 & 0 & 0 & 0 & -f_{N-2} & g_{N-1} \end{bmatrix} \begin{Bmatrix} T_{2,j} \\ T_{3,j} \\ T_{4,j} \\ T_{5,j} \\ ... \\ T_{N-1,j} \end{Bmatrix} = \begin{pmatrix} \overline{z_1} \\ z_2 \\ z_3 \\ z_4 \\ ... \\ \overline{z_{N-2}} \end{pmatrix}. \tag{25}$$

where

$$\overline{z_1} = f_1 T_{1,j} + l_2 T_{2,j} + s_3 T_{3,j} + f_1 T_{1,j+1}, \tag{26}$$

$$z_2 = f_2 T_{2,j} + l_3 T_{3,j} + s_4 T_{4,j}, \tag{27}$$

$$z_3 = f_3 T_{3,j} + l_4 T_{4,j} + s_5 T_{5,j}, \tag{28}$$

$$\overline{z_{N-2}} = f_{N-2} T_{N-2,j} + l_{N-1} T_{N-1,j} + s_N T_{N,j} + f_N T_{N,j+1}. \tag{29}$$

The algebraic equation system given by Eq. (25) is solved for all time steps $j=1,2,...,M$. The parameters in coefficient matrix are not constants since they depend on the material properties in FGM layer. In Eqs (26) - (29), $T_{1,j+1}$ and $T_{N,j+1}$ are known temperature values from the specified boundary conditions. The algebraic equation system is solved for unknown temperatures at interior points.

4.3. Finite element method (FEM)

The parametric finite element analyses are performed with ANSYS Parametric Design Language (APDL) [29]. 8-node PLANE77 element is utilized in simulations. This element is a higher order version of the 2-D, 4-node thermal element PLANE55 [29]. The element has one degree of freedom which is temperature at each node. The 8-node thermal element is appropriate to a 2-D, steady-state or transient thermal analyses. The geometry, node locations and the coordinate system for PLANE77 is depicted in Fig 3(a). A triangular shape option may be formed by merging three nodes at the same point. Modelling functionally graded layer using finite elements requires assigning continuously varying material properties into the layer. The most conventional way to model graded material inhomogeneity involves the use of conventional homogenous elements in successive layers of the mesh, containing own material properties [30]. Hence, stepwise change in properties along the direction of gradation is satisfied. Such ways have already been used for many researchers [31-32], hence we have

adopted this model in the present study. Constructed finite element mesh for transient heat conduction analysis of the FGM layer is depicted in Fig. 3(b).

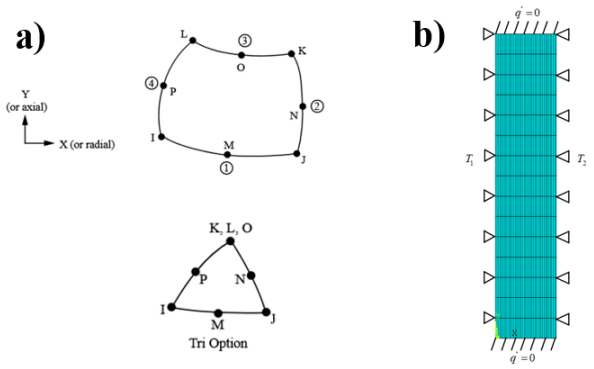

Fig. 3. (a) Two-dimensional 8-node thermal solid element available in ANSYS [29] (b) Constructed finite element mesh for the FGM layer

5. Results

In this section, we provide temperature distribution results. Firstly, obtained results based on three different methods are compared with each other to verify the developed numerical formulations. Two different boundary and initial conditions are applied to the layer and they are labeled as Case 1 and Case 2 as mentioned in section 2. In Case 1, the temperature at left and right surfaces of the layer is kept constant as 0 K and FGM layer is loaded by a sinusoidal temperature profile initially. In Case 2, the temperature at left surface of FGM layer is kept constant as $2T_0$ K whereas the temperature at right surface is kept constant as T_0 K. In both cases, the influences of inhomogeneity constants for thermal conductivity, mass density and thermal capacitance on transient temperature distribution in an FGM layer are examined. Before analyzing the effect of inhomogeneity constants, the temperature distribution in the FGM layer is analyzed and compared with that obtained in a homogeneous layer which is composed of 100% Ti-6Al-4V. Fig. 7(a) and 7(b) respectively show the contours of temperature distribution in homogenous layer and FGM layer in Case 1 condition with respect to time. Temperature values in the layer is normalized utilizing $T_0 = 1000K$. Hence, $T(x)/T_0$ results are presented in parametric studies. The coordinate parameter along the layer is normalized by the following equation,

$$\bar{x} = \frac{2x}{L} - 1. \tag{30}$$

According to these figures, the homogenous layer is cooling faster than the FGM layer. Moreover, cooling in homogenous layer appears symmetric whereas cooling in FGM layer appears not symmetric as predicted. Since right surface of the layer composed of ZrO_2, conduction towards right surface gradually decreases. The low thermal conductivity of ZrO_2 plays an important role on observing such a behavior. Fig. 7(c) and (d) show the contours of temperature distribution of homogenous layer and FGM layer, respectively when Case 2 condition is applied to the layer. When Figs 7(c) and (d) are examined, temperature at the right surface of homogenous layer diffuses faster into the thickness of the layer when compared to that of FGM layer. Therefore, the cool region emerging around the metallic surface of FGM layer is larger than that of homogenous layer.

Fig.8 (a) and (b) show the temperature distribution in a homogenous layer loaded by Case 1 and Case 2 conditions with respect to time for the discussed numerical methods. It can be inferred from figures that results of developed code for explicit and implicit schemes are in a very good agreement with those of finite element analysis. In addition, Fig.9 (a) and (b) illustrate the temperature distribution in a functionally graded layer loaded by Case 1 and Case 2 conditions with respect to time. Since layer is made of FGM, cooling curves observed from Fig. 9(a) is not symmetric, and heating curves appearing in Fig. 9(b) is different from that appearing in Fig. 8(b). It can be inferred from Fig. 9(a) and (b) that obtained results for the FGM layer are in a very good agreement with the results of finite element method similar to the homogeneous case.

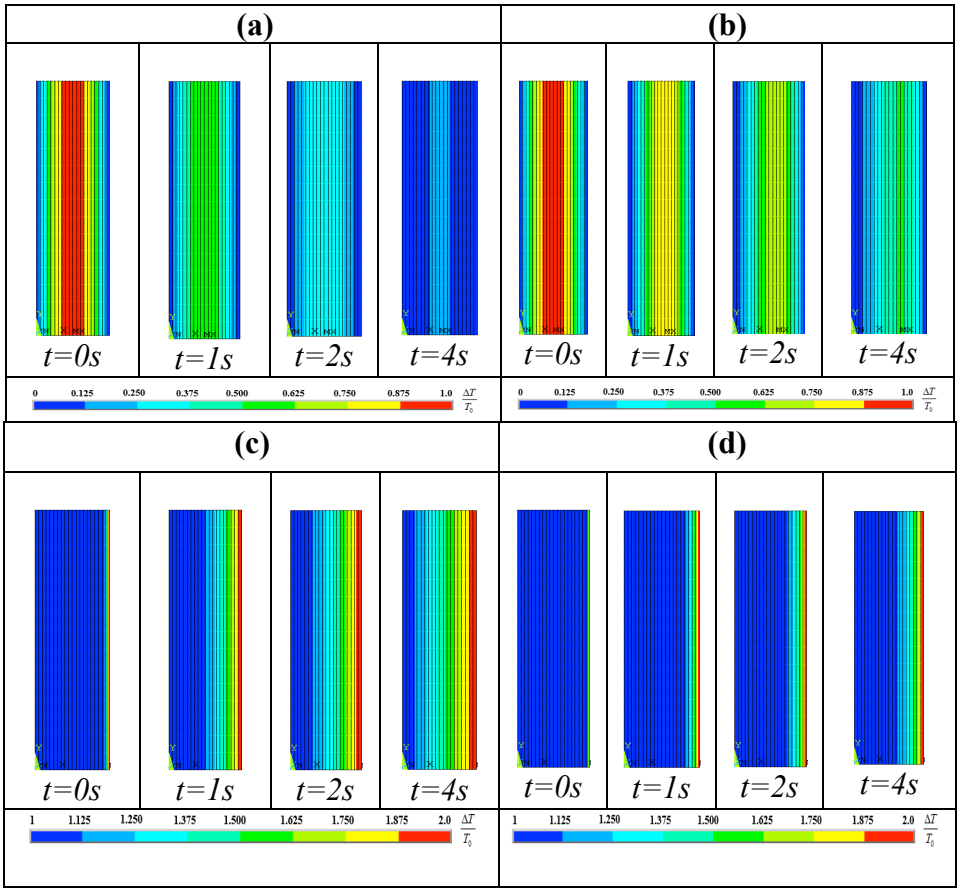

Fig. 7. (a) Temperature contours in homogenous layer in Case 1, (b) Temperature contours in FGM layer in Case 1, (c) Temperature contours in homogenous layer in Case 2, (d) Temperature contours in FGM layer in Case 2.

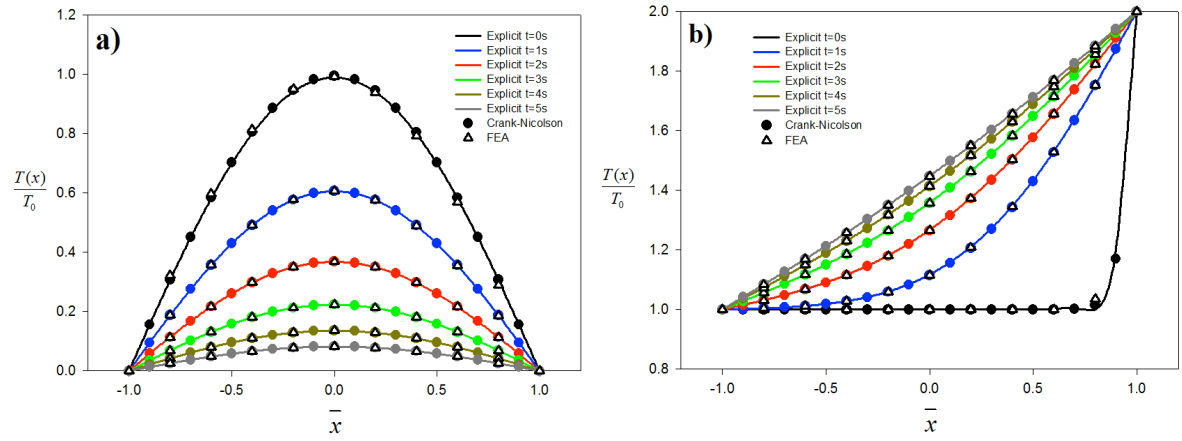

Fig. 8. Temperature distribution in homogenous layer made of Ti-6Al-4V using different numerical techniques with respect to time $\gamma_1 = 0, \gamma_2 = 0, \gamma_3 = 0$.

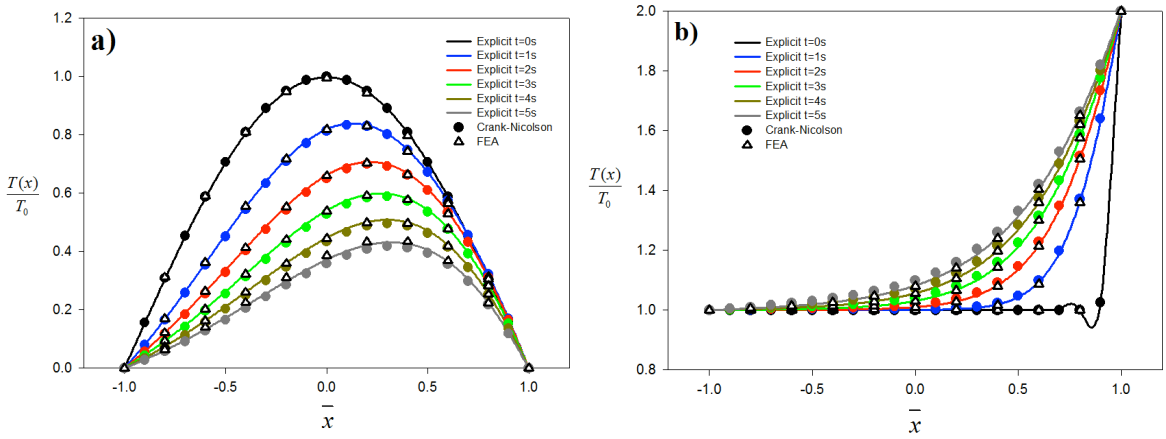

Fig. 9. Temperature distribution in FGM layer made of Ti-6Al-4V and ZrO_2 using different numerical techniques with respect to time $\gamma_1 = -2.185, \gamma_2 = -0.2724, \gamma_3 = 0.2366$.

The influence of each inhomogeneity constants on the temperature distribution is evaluated and compared with each other. This is performed by analyzing the temperature at the midpoint of the layer ($T_{MP} = T(x/2)$) while varying each inhomogeneity parameter, individually. Fig. 16 shows the variation of normalized temperature with respect to time for the midpoint of the layer. Shown in Figs. 10 (a)-(d), the midpoint temperature is decreasing with time under Case 1 condition whereas it is increasing under Case 2 condition. For both cases, the variation $\gamma_2 L$ and $\gamma_3 L$ have similar influences and increase in those parameters results in higher midpoint temperature while cooling condition in Case 1 and lower midpoint temperature while heating condition in Case 2. Furthermore, the opposite is true for the increase in $\gamma_1 L$. Decrease in $\gamma_2 L$ and $\gamma_3 L$ leads to lower midpoint temperature in Case 1 in which cooling occurs and much higher midpoint temperature in Case 2 where heating happens. On the contrary, decrease in $\gamma_1 L$ causes higher midpoint temperature in Case 1 and lower temperature in Case 2. The main reason behind this behavior is that the inhomogeneity constant solely participate in transient heat conduction Eq. (5) ahead of $\frac{\partial T}{\partial x}$ term and γ_1 exponentially contributes to the thermal diffusivity (see Eq. (6)) in a positive way, however

the opposite is true for γ_2 and γ_3. Following figure (see Fig. 11) illustrates the midpoint temperature when inhomogeneity constants $\gamma_1 L$, $\gamma_2 L$ and $\gamma_3 L$ are varied together. Hence, combined effect of inhomogeneity parameters on midpoint temperature value can be clearly observed. When $\gamma_1 L$, $\gamma_2 L$ and $\gamma_3 L$ are increased together, the midpoint temperature in Case 1 rises and Case 2 reduces. Similarly, decrease in $\gamma_1 L$, $\gamma_2 L$ and $\gamma_3 L$ together leads to lower midpoint temperature value in Case 1 and higher midpoint temperature value in Case 2. We can draw such a conclusion from the findings that the alteration of $\gamma_2 L$ and $\gamma_3 L$ are more dominant on midpoint temperature value in layer than that of $\gamma_1 L$.

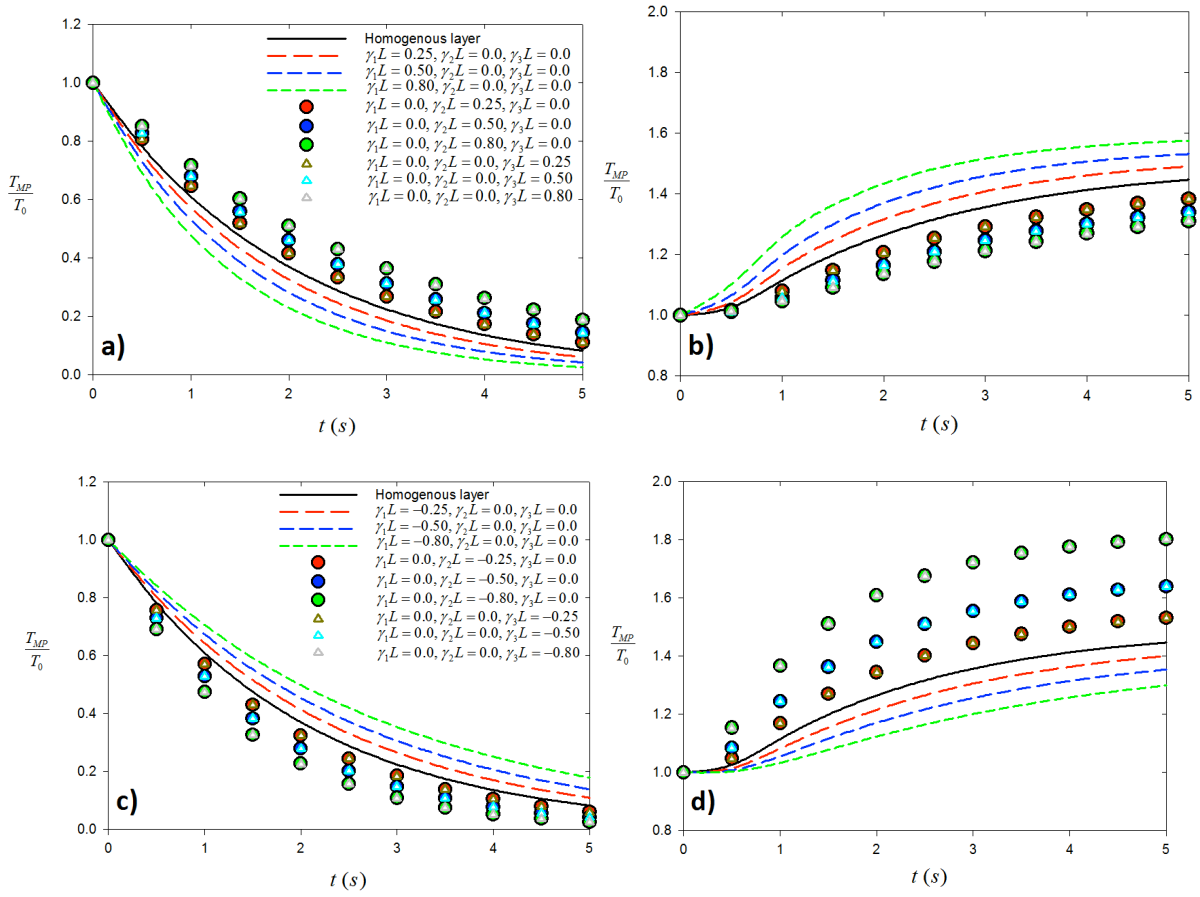

Fig. 10. The midpoint temperature value in FGM layer with respect to time (a) for increasing values of inhomogeneity constants $\gamma_1 L, \gamma_2 L$ and $\gamma_3 L$ individually (a) Case 1 (b) Case 2; (c) for decreasing values of inhomogeneity constants $\gamma_1 L, \gamma_2 L$ and $\gamma_3 L$ individually (c) Case 1 (d) Case 2.

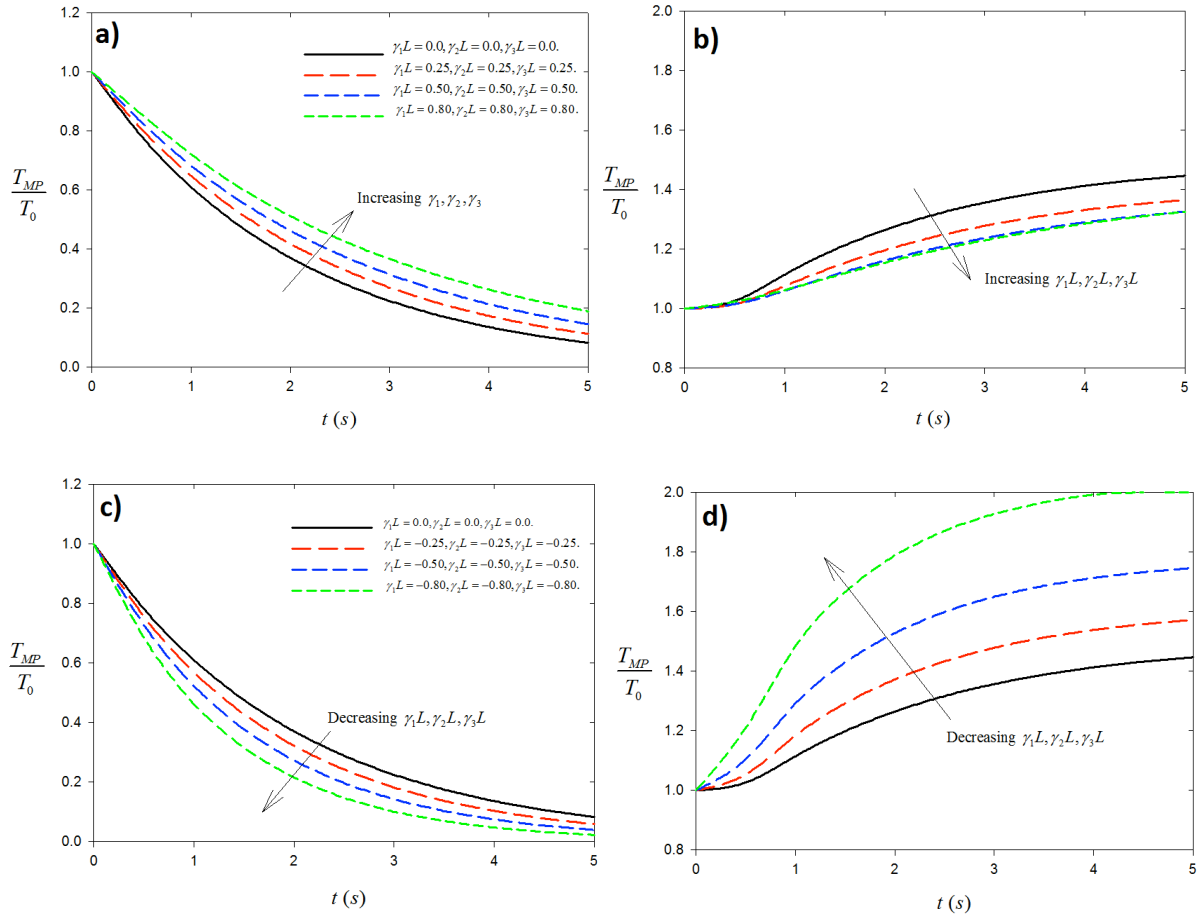

Fig. 11. The midpoint temperature value in FGM layer with respect to time (a) for increasing values of $\gamma_1 L, \gamma_2 L$ and $\gamma_3 L$ together in Case 1 (b) for increasing values of $\gamma_1 L, \gamma_2 L$ and $\gamma_3 L$ together in Case 2 (c) for decreasing values of $\gamma_1 L, \gamma_2 L$ and $\gamma_3 L$ together in Case 1 (d) for decreasing values of $\gamma_1 L, \gamma_2 L$ and $\gamma_3 L$ together in Case 2.

In order to see which of the inhomogeneity parameter is the most dominant, the normalized values of midpoint temperature in the layer at t=5s are provided in Table 3. Midpoint temperatures regarding individual and combined alteration of the inhomogeneity constants are given in a tabular format. Percent difference is shown by $\varepsilon\%$ and it is calculated with respect to the temperature in which combined inhomogeneity take place ($\gamma_1 L = \gamma_2 L = \gamma_3 L = 0.8$ and $\gamma_1 L = \gamma_2 L = \gamma_3 L = -0.8$). We have denoted this temperature using (*) as the referencing state. In Case 1 and 2, when dimensionless temperature values are compared, increase in $\gamma_2 L$ and $\gamma_3 L$ have equal influence on temperature and they lead to get closer temperatures to the temperature at referencing state. For both cases, decreases in $\gamma_2 L$ and $\gamma_3 L$ have the same effect and they are more influential than the change in $\gamma_1 L$. It can be quantitatively inferred from Table 3 that the inhomogeneity constants $\gamma_2 L$ and $\gamma_3 L$ have greater influence on midpoint temperature than that of $\gamma_1 L$ and they equally influence the temperature value.

Table 3. Normalized midpoint temperature values at t=5s.

	Case 1 $T_{MP}/T_0\,(t=5s)$	ε%	**Case 2** $T_{MP}/T_0\,(t=5s)$	ε%
Homogenous Layer	0.08291	56.23	1.44732	9.13
$\gamma_1 L=0.8, \gamma_2 L=0.0, \gamma_3 L=0.0.$	0.02573	86.41	1.57624	18.85
$\gamma_1 L=0.0, \gamma_2 L=0.8, \gamma_3 L=0.0.$	0.18846	0.517	1.30999	1.22
$\gamma_1 L=0.0, \gamma_2 L=0.0, \gamma_3 L=0.8.$	0.18846	0.517	1.30999	1.22
$\gamma_1 L=0.8, \gamma_2 L=0.8, \gamma_3 L=0.8.$	**0.18944(*)**	-	**1.32623(*)**	-
$\gamma_1 L=-0.8, \gamma_2 L=0.0, \gamma_3 L=0.0.$	0.17870	712.02	1.29911	35.05
$\gamma_1 L=0.0, \gamma_2 L=-0.8, \gamma_3 L=0.0.$	0.02523	14.06	1.80274	9.86
$\gamma_1 L=0.0, \gamma_2 L=0.0, \gamma_3 L=-0.8.$	0.02523	14.06	1.80274	9.86
$\gamma_1 L=-0.8, \gamma_2 L=-0.8, \gamma_3 L=-0.8.$	**0.02212(*)**	-	**2.00000(*)**	-

6. Conclusions

In this study, the transient heat conduction in a functionally graded layer is examined using various computational techniques. Heat conduction equation for the functionally graded layer is derived without any simplification for the inhomogeneity. Hence, inhomogeneity parameters controlling thermal conductivity, specific heat capacitance and mass density involve. Time dependent temperature distribution in the functionally graded layer is obtained by applying explicit and implicit schemes to the time dependent variable coefficient partial differential equation (PDE). Developed formulations for the functionally graded layer are implemented via computer codes in MATLAB. In addition, functionally graded layer is modeled in ANSYS [29] and transient heat conduction analysis is carried out. Two different cases of boundary and initial conditions are considered. In the first case, the layer is loaded by the sinusoidal temperature initially while temperatures at surfaces of the layer are kept constant, so cooling behavior is observed. In the second case, one of the surfaces of the layer is subjected to $2T_0$ K while other surface is hold at T_0 K, hence heating behavior is seen. In both cases, the results of developed formulations are compared with those obtained by finite element analysis and a very good agreement is accomplished. Then, a series of parametric analyses are conducted to investigate the separate effects of inhomogeneity constants on temperature distributions. The results of this study can guide the material specialists to determine the materials to be utilized in an FGM layer in thermal barriers according to the desired temperature distribution. Some concluding remarks are summarized as follows:

- Decrease in $\gamma_1 L$ leads to higher temperatures towards the ceramic side in an FGM layer.
- The change in $\gamma_2 L$ and $\gamma_3 L$ affects the temperature in an equal manner. Increase in $\gamma_2 L$ and $\gamma_3 L$ leads to slow temperature change whereas decrease in those parameters causes a fast change.

- The order of the dominance of the inhomogeneity constants on thermal conductance analysis is summarized as: $\gamma_2 L = \gamma_3 L > \gamma_1 L$.

References

[1] Miyamoto, Y., Kaysser, W.A., Rabin, B.H., Kawasaki, A., Ford, R.G., Functionally Graded Materials Design, Processing and Applications. Springer Science & Business Media, New York 1999.

[2] Naebe, M., Shirvanimoghaddam, K., Functionally graded materials: A review of fabrication and properties. *Applied Materials Today*, 5, 223-245, 2016.

[3] Bellur-Ramaswamy, R.S., Haber, R., Sobh, N.A., Tortorelli, D.A., Modelling and process optimization for functionally graded materials. *International Journal for Numerical Methods in Engineering*, 62, 186-204, 2005.

[4] Fukui, Y., Takashima, K., Ponton, C.B., Measurement of Young's modulus and internal friction of an in situ Al-Al_3Ni functionally gradient material. *Journal of Materials Science*, 29(9), 2281-2288, 1994.

[5] Abbas, M.R., Uday, M.B., Noor, A.M., Ahmad, N., Rajoo, S., Microstructural evaluation of a slurry based Ni/YSZ thermal barrier coating for automotive turbocharger turbine application. *Materals & Design*, 109, 47-56, 2016.

[6] Dhineshkumar, S.R., Duraiselvam, M., Natarajan, S., Panwar, S.S., Jena, T., Khan, M.A., Enhancement of strain tolerance of functionally graded $LaTi_2Al_9O_{19}$ thermal barrier coating through ultra-short pulsed based laser texturing. *Surface & Coatings Technology*, 304, 263-271, 2016.

[7] Naga, S.M., Awaad, M., El-Maghraby, H.F., Hassan, A.M., Elhoriny, M., Killinger, A., Gadow, R., Effect of $La_2Zr_2O_7$ coat on the hot corrosion of multi-layer thermal barrier coatings. Materials & Design, 102, 1-7, 2016.

[8] Daikh, A.A., Megueni, A., Thermal behavior of Functionally Graded Materials. *In: 5th International Conference on Welding Non Destructive Testing and Materials and Alloys Industry*, Oran, Algeria, 2016.

[9] Kuroda, Y., Kusaka, K., Moro, A., Togawa, M., Evaluation tests of ZrO_2/Ni functionally gradient materials for regeneratively cooled thrust engine applications. Holt J.B., Koizumi M., Hirai T., Munir Z.A. (Eds.), *Ceramic Transactions*, 34, Functionally Gradient Materials, American Ceramic Society, Westerville, Ohio, 289-296, 1993.

[10] Reddy, J.N., Chin, C.D., Thermomechanical analysis of functionally graded cylinders and plates. *Journal of Thermal Stresses*, 21(6), 593-626, 1998.

[11] Yang, Y., Temperature Dependent Thermoelastic Analysis of Multi-dimensional Functionally Graded Materials, Ph.D. Dissertation, University of Pittsburgh, USA, 2015.

[12] Hosseini, S.M., Akhlaghi, M., Shakeri, M., Transient heat conduction in a functionally graded thick hollow cylinders by analytical method. *Heat and Mass Transfer*, 43, 669-675, 2007.

[13] Bahtui, A., Eslami, M.R., Generalized coupled thermoelasticity of functionally graded cylindrical shells. *International Journal for Numerical Methods in Engineering*, 69, 676-697, 2007.

[14] Zhao, X., Liew, K.M., An element-free analysis of mechanical and thermal buckling of functionally graded conical shell panels. *International Journal for Numerical Methods in Engineering*, 86, 269-285, 2011.

[15] Sharma, R., Jadon, V.K., Singh, B., Analysis of temperature field in a composite functionally graded material plate by finite element method. *International Journal of Advances in Materials Science and Engineering (IJAMSE)*, 4(4), 41-47, 2015.

[16] Cho, J.R., Oden, J.T., Functionally graded material: a parametric study on thermal-stress characteristics using the Crank-Nicolson-Galerkin scheme. *Computer Methods in Applied Mechanics and Engineering*, 188, 17-38, 2000.

[17] Nemat-Alla, M., Reduction of thermal stresses by composition optimization of two-dimensional functionally graded materials. *Acta Mechanica*, 208, 147-161, 2009.

[18] Sladdek, J., Sladdek, V., Zhang, C., Transient heat conduction analysis in a functionally graded materials by the meshless local boundary integral equation method. *Computational Materials Science*, 28, 494-504, 2003.

[19] Sadowski, T., Nakonieczny, K., Thermal shock response of FGM cylindrical plates with various grading patterns. *Computational Materials Science*, 43: 171-178, 2008.

[20] Nakonieczny, K., Sadowski, T., Modelling of 'thermal shocks' in composite materials using meshfree FEM. *Computational Materials Science*, 44, 1307-1311, 2009.

[21] Li, G., Guo, S., Zhang, J., Li, Y., Han, L., Transient heat conduction analysis of functionally graded materials by a multiple reciprocity boundary face method. *Engineering Analysis with Boundary Elements*, 60, 81-88, 2015.

[22] Li, M., Wen, P.H., Finite block method for transient heat conduction analysis in functionally graded media. *International Journal for Numerical Methods in Engineering*, 99, 372-390, 2014.

[23] Olatunji-Ojo, A.O., Boetcher, S., Cundari, T.R., Thermal conduction analysis of layered functionally graded materials. *Computational Materials Science*, 54, 329-335, 2012.

[24] Jin, Z., Heat Conduction in a Functionally Graded Plate Subjected to Finite Cooling/Heating Rates: An Asymptotic Solution. *Materials*, 4(12), 2108-2118, 2011.

[25] Chan, Y-S., Paulino, G.H., Fannjiang, A.C., Gradient Elasticity Theory for Mode III Fracture in Functionally Graded Materials – Part II: Crack Parallel to the Material Gradation. *ASME Journal of Applied Mechanics*, 75(0611015), 1-11, 2008.

[26] Balci, M.N., Dag, S., Yildirim, B., Subsurface stresses in graded coatings subjected to frictional contact with heat generation. *Journal of Thermal Stresses*, 40(4), 517-534, 2017.

[27] Chen, P., Chen, S., Thermo-mechanical contact behavior of a finite graded layer under a sliding punch with heat generation. *International Journal of Solids and Structures*, 50, 1108-1119, 2013.

[28] Fujimoto, T., Noda, N., Influence of the compositional profile of functionally graded material on the crack path under thermal shock. *Journal of the American Ceramic Society*, 84(7), 1480-1486, 2001.

[29] ANSYS, ANSYS Basic Analysis Procedures Guide, release 15.1, ANSYS Inc., Canonsburg, PA, USA, 2015.

[30] Burlayenko, V.N., Altenbach, H., Sadowski, T., Dimitrova, S.D., Bhaskar, A., Modelling functionally graded materials in heat transfer and thermal stress analysis by means of graded finite elements. *Applied Mathematical Modelling*, 45,422-438, 2017.

[31] Fuchiyama, T., Noda, N. Analysis of thermal stresses in a plate of functionally gradient material. *JSAE Review*, 16, 373-387, 1995.

[32] Anlas, G., Santare, N.H., Lambros, J., Numerical calculation of stress intensity factors in a functionally graded materials. *International Journal of Fracture*, 104, 131-143, 2000.

International Journal of Engineering & Applied Sciences (IJEAS)
Vol.11, Issue 3 (2019) 445-454
http://dx.doi.org/10.24107/ijeas.641211
Int J Eng Appl Sci 11(3) (2019) 445-454

Geometric Mapping for Non-Rectangular Plates with Micro/Nano or Macro Scaled under Different Effects

Kadir Mercan [a], *Ömer Civalek* [b*]

[a,b]Akdeniz University, Civil Engineering Dept., Antalya / TURKIYE

E-Mail address: kmercan@mehmetakif.edu.tr [a], civalek@yahoo.com [b*]

ORCID numbers of authors:
0000-0003-3657-6274[a], *0000-0003-1907-9479*[b]

Received date: 10.10.2019
Accepted date: 08.11.2019

Abstract

The main purpose of this study is to give a perspective via discrete singular convolution, differential quadrature (DQ) and harmonic differential quadrature (HDQ). For this purpose, DQ and HDQ methods are developed for the buckling, analysis of non-rectangular plates. Plates of, skew, shape is considered under axial loads. Furthermore, transformation formulations and some perspective for nano or macro scaled many problems with different effects discussed via discrete singular convolution and differential quadrature methods.

Keywords*:* Discrete singular convolution, Harmonic differential quadrature; Plates; Graphene sheet, nonlocal elasticity, buckling.

1. Introduction

It is well known that, the analysis of engineering systems includes two main stages, such as; construction of a mathematical model for a given physical phenomena and the solution of this mathematical equation. Real physical systems or engineering problems are often described by partial differential equations, either linear or nonlinear and in most cases, their closed form solutions are extremely difficult to establish. As a result, approximate numerical methods have

been widely used to solve partial differential equations that arise in almost all engineering disciplines. The most commonly used numerical methods for such applications are the finite element, finite difference, Ritz, and boundary element method, and most engineering problems can be solved by these methods to adequate accuracy if a proper and sufficient number of grid points are used. In addition to this, in a large number of practical applications where only reasonably accurate solutions at few specified physical coordinates are of interest, the conventional numerical methods such as finite element or finite difference method require a large number of grid points and so large a computer capacity. Among a variety of numerical methods, the finite element method is by far the most effectively and widely used method. Furthermore, finite element method is still an effective method in especially the systems with complex geometry and load conditions or applications with non-linear behavior and it has many successful applications. In seeking a more efficient numerical method that requires fewer grid points yet achieves acceptable accuracy, the method of differential quadrature (DQ) was introduced by Bellman et al. [1]. Since then, applications of differential quadrature method to various engineering problems have been investigated and their successes have demonstrated the potential of the method as an attractive numerical analysis technique [2-10]. The stability analysis of plates may be either closed form or approximate. The closed form solutions consist of techniques for seeking direct solutions to the governing differential equation of plates. A closed form or rigorous solution of plates can be obtained for only a limited number of cases. For the majority of practical problems, a closed form namely analytical solution either cannot be obtained or is of such a complicated nature that it can be applied only with great difficulty in a practical computation. For many situations, numerical methods are the only approaches that can be employed [11-17].

The focus of this paper is on the comparison study of the DQ and HDQ methods. For this reason, the applications are limited to those problems having smooth solutions for simplicity. In addition to this, since the only thin plates are considered in this paper, there are some assumptions regarding the behavior of thin plates. These are; the transverse deflections of the plates are small compared to the thickness of the plate. Thus middle-surface stretching caused by bending can be neglected; that is, membrane action resulting from flexure is negligible compared to the flexure. The material of the plate is homogeneous, isotropic, and obeys Hooke's law.

2. Differential Quadrature Method (DQM)

For simplicity, we consider a one-dimensional function $u(x)$ in the [-1,1] domain, and N discrete points. Then the first derivatives at point i, at $x = x_i$ is given by

$$u_x(x_i) = \left.\frac{\partial u}{\partial x}\right|_{x = x_i} = \sum_{j=1}^{N} A_{ij}\, u(x_j) \quad ; \quad i = 1,2,.....,N \tag{1}$$

where x_j are the discrete points in the variable domain, $u(x_j)$ are the function values at these points and A_{ij} are the weighting coefficients for the first order derivative attached to these function values. Bellman et al. [1,2] suggested two methods to determine the weighting coefficients. The first one is to let equation (1) be exact for the test functions

$$u_k(x) = x^{k-1}; \; k = 1,2,...,N \tag{2}$$

which leads to a set of linear algebraic equations

$$(k-1)\, x_i^{k-2} = \sum_{j=1}^{N} A_{ij}\, x_j^{k-1}; \text{ for } \; i = 1,2,.....,N \quad \text{and} \quad k = 1,2,.....,N \tag{3}$$

which represents N sets of N linear algebraic equations. Thus, the weighting coefficients for each formula will be different from those for the first order derivative. As similar to the first order, the second order derivative can be written as

$$u_{xx}(x_i) = \left.\frac{\partial^2 u}{\partial x^2}\right|_{x=x_i} = \sum_{j=1}^{N} B_{ij}\, u(x_j) \quad ; \quad i = 1,2,.....,N \tag{4}$$

where the B_{ij} is the weighting coefficients for the second order derivative.

Another way to determine the weighting coefficients is to employ harmonic functions, named the harmonic differential quadrature (HDQ). Harmonic differential quadrature has been proposed by Striz et al. [19]. Unlike the differential quadrature that uses the polynomial functions, such as power functions, Lagrange interpolated, and Legendre polynomials as the test functions, harmonic differential quadrature uses harmonic or trigonometric functions as the test functions. Thus, this method is called the HDQ method. Shu and Xue proposed an explicit means of obtaining the weighting coefficients for the HDQ [18]. The harmonic test function $h_k(x)$ used in this approach is defined as;

$$h_k(x) = \frac{\sin\frac{(x-x_0)\pi}{2}\cdots\cdots\sin\frac{(x-x_{k-1})\pi}{2}\sin\frac{(x-x_{k+1})\pi}{2}\cdots\cdots\sin\frac{(x-x_N)\pi}{2}}{\sin\frac{(x_k-x_0)\pi}{2}\cdots\cdots\sin\frac{(x_k-x_{k-1})\pi}{2}\sin\frac{(x_k-x_{k+1})\pi}{2}\cdots\cdots\sin\frac{(x_k-x_N)\pi}{2}}$$

$$\text{for} \quad k = 0,1,2,....,N \tag{5}$$

According to the HDQ, the weighting coefficients of the first-order derivatives A_{ij} for $i \neq j$ can be obtained by using the following formula:

$$A_{ij} = \frac{(\pi/2)P(x_i)}{P(x_j)\sin[(x_i - x_j)/2]\pi}, \qquad i,j = 1,2,3,.....,N \tag{6}$$

where

$$P(x_i) = \prod_{j=1, j\neq i}^{N} \sin\left(\frac{x_i - x_j}{2}\pi\right), \quad \text{for j = 1,2,3,.....N} \tag{7}$$

The weighting coefficients of the second-order derivatives B_{ij} for $i \neq j$ can be obtained using following formula:

$$B_{ij} = A_{ij}\left[2A_{ii}^{(1)} - \pi ctg\left(\frac{x_i - x_j}{2}\right)\pi\right], \qquad i,j = 1,2,3,.....,N \tag{8}$$

3. Applications of DQ methods

The governing differential equations for skew plates under uniaxial compression (uniform normal force) F_x along the x direction and its differential quadrature form are given respectively,

$$u_{xxxx} - (4k\cos\theta)u_{xxxy} + 2k^2(1+2\cos^2\theta)u_{xxyy} - (4k^3\cos\theta)u_{xyyy} + k^4 u_{yyyy} = -\frac{a^2}{D}F_x \sin^4(\theta/4)u_x \tag{9}$$

$$\sum_{n=1}^{N_x} D_{in}u_{nj} - 4k\cos\theta \sum_{n=1}^{N_x} C_{in} \sum_{m=1}^{N_y} A_{jm}u_{mn} + 2k^2(1+2\cos^2\theta) \sum_{n=1}^{N_x} B_{in} \sum_{m=1}^{N_y} B_{jm}u_{im}$$

$$-2k^2(1+2\cos^2\theta) \sum_{n=1}^{N_x} A_{in} \sum_{m=1}^{N_y} C_{jm}u_{mn} + k^2 \sum_{m=1}^{N_y} D_{jm}u_{mi} = \frac{a^2}{D}F_x \sin^4(\theta/4) \sum_{n=1}^{N_x} A_{in}u_{mj} \tag{10}$$

$$i = 1,2,.....,N_x \quad \text{and} \quad j = 1,2,.....,N_y$$

where θ is skew angle, $k = a/b$ is the aspect ratio, u is the displacement in the z direction, and D is the flexural rigidity. Clamped support condition with movable edges is considered. In accordance with this condition the plate is prevented from moving in the z direction or rotating at

the boundaries. In this case both the deflection and slope must vanish. Since the first and last displacements are known, Eq. (36) is rewritten for boundary conditions

$$\sum_{n=1}^{N_x} D_{in} u_{nj} - 4k\cos\theta \sum_{n=1}^{N_x} C_{in} \sum_{m=1}^{N_y} A_{jm} u_{mn} + 2k^2(1+2\cos^2\theta) \sum_{n=1}^{N_x} B_{in} \sum_{m=1}^{N_y} B_{jm} u_{im}$$

$$-2k^2(1+2\cos^2\theta) \sum_{n=1}^{N_x} A_{in} \sum_{m=1}^{N_y} C_{jm} u_{mn} + k^2 \sum_{m=1}^{N_y} D_{jm} u_{mi} = \frac{a^2}{D} F_x \sin^4(\theta/4) \sum_{n=1}^{N_x} A_{in} u_{mj} \tag{11}$$

$i = 2,.....,N_x$ -1 and $j = 2,.....,N_y$-1

Consequently, we solve the remaining eigenvalue problem to obtain the buckling loads.

4. Discrete Singular Convolution (DSC)

Wei [18-20] proposed the method of discrete singular convolution (DSC) in 1998. In this method, numerical solutions of differential equations are discrete via some kernels. A singular convolution defined below [19]

$$F(t) = (T * \eta)(t) = \int_{-\infty}^{\infty} T(t-x)\eta(x)dx \tag{12}$$

For example, regularized Shannon kernel (RSK) is more suitable for practical applications. This kernel can write as follows [18]

$$\delta_{\Delta,\sigma}(x - x_k) = \frac{\sin[(\pi/\Delta)(x-x_k)]}{(\pi/\Delta)(x-x_k)} \exp\left[-\frac{(x-x_k)^2}{2\sigma^2}\right];\ \sigma>0 \tag{13}$$

by using the method of DSC and DQ methods plates with different shape can be solve via below transformation rules

$$\frac{\partial^2 w}{\partial x^2} = [J_{22}]^{-1} \sum_{i=-M}^{M} \delta^{(2)}{}_{\Delta,\sigma}(k\Delta\xi) w_{ik} - [J_{22}]^{-1}[J_{21}][J_{11}]^{-1} \sum_{i=-M}^{M} \delta^{(1)}{}_{\Delta,\sigma}(k\Delta\xi) w_{ik} \tag{14a}$$

$$\frac{\partial^2 w}{\partial y^2} = [J_{22}]^{-1} \sum_{i=-M}^{M} \delta^{(2)}{}_{\Delta,\sigma}(k\Delta\eta) w_{jk} - [J_{22}]^{-1}[J_{21}][J_{11}]^{-1} \sum_{i=-M}^{M} \delta^{(1)}{}_{\Delta,\sigma}(k\Delta\eta) w_{jk} \tag{14b}$$

$$\frac{\partial^2 w}{\partial x \partial y} = [J_{22}]^{-1} \sum_{i=-M}^{M} \delta^{(1)}{}_{\Delta,\sigma}(k\Delta\xi) \sum_{i=-M}^{M} \delta^{(1)}{}_{\Delta,\sigma}(k\Delta\eta) w_{ij}$$

$$- [J_{22}]^{-1}[J_{21}][J_{11}]^{-1} \sum_{i=-M}^{M} \delta^{(1)}{}_{\Delta,\sigma}(k\Delta\eta) w_{jk} \tag{15}$$

$$\Theta_x^n(\,) = \frac{\partial^{(n)}(\,)}{\partial x^{(n)}} = \sum_{k=-M}^{M} \delta^{(n)}_{\Delta,\sigma}(k\Delta x)(\,)_{i+k,j} \tag{16}$$

$$\Theta_y^n(\,) = \frac{\partial^{(n)}(\,)}{\partial y^{(n)}} = \sum_{k=-M}^{M} \delta^{(n)}_{\Delta,\sigma}(k\Delta y)(\,)_{i,j+k} \tag{17}$$

$$\Theta_x^1 \Theta_y^{(n-1)}(\,) = \frac{\partial^{(n)}(\,)}{\partial x \partial y^{(n-1)}} = \sum_{k=-M}^{M} \delta^{(1)}_{\Delta,\sigma}(k\Delta x)(\,)_{i+k,j} \sum_{k=-M}^{M} \delta^{(n-1)}_{\Delta,\sigma}(k\Delta y)(\,)_{i,k+j} \tag{18}$$

$$\Theta_x^{(n-1)} \Theta_y^1(\,) = \frac{\partial^{(n)}(\,)}{\partial x^{(n-1)} \partial y} = \sum_{k=-M}^{M} \delta^{(n-1)}_{\Delta,\sigma}(k\Delta x)(\,)_{i+k,j} \sum_{k=-M}^{M} \delta^{(1)}_{\Delta,\sigma}(k\Delta y)(\,)_{i,k+j} \tag{19}$$

Similar transformation can also possible for DQ or HDQ methods.

5. Concluding remarks and nano-scaled plates

In the applied mechanics area, many different problems can be solved via DSC or DQ transformation methods. For example, below cases can be consider for each plate problem (triangular, skew, trapezoidal, circular, annular, sector, polygonal, deltoid, or general non-rectangular plates:

5.1. Foundation effects, magnetic effects, piezo effect.

5.2. Functionally graded (FG) composite material
5.3. CNT reinforced composite material
5.4. Graphene platelet reinforced composite material
5.5. Nonlinear analysis-material nonlinearity
5.6. Buckling
5.7. Bending
5.8. Vibration
5.9 Porosity effect
5.10. Post buckling
5.11. Nonlinear analysis-geometric nonlinearity
5.12. Viscoelasticity, damped vibration.

Also, micro/nano scaled plates, beam and shell problems can also be solved [21-31] via these methods.

References

[1] Bellman, R., Casti, J., Differential quadrature and long-term integration, *Journal of Mathematical Analysis and Application,* 34, 235-38, 1971.

[2] Bellman, R., Kashef, B.G., Casti, J., Differential Quadrature: A technique for the rapid solution of nonlinear partial differential equation, *Journal of Computational Physics,* 10, 40-52, 1972.

[3] Bert, C.W., Malik, M., The differential quadrature method for irregular domains and application to plate vibration, *International Journal of Mechanical Science*, 38(6), 589-606, 1996.

[4] Bert, C.W., Jang, S.K., Striz, A.G., Two new approximate methods for analyzing free vibration of structural components, *AIAA Journal*, 26(5), 612-18, 1987.

[5] Bert, C.W., Wang, Z., Striz, A.G., Differential quadrature for static and free vibration analysis of anisotropic plates, *International Journal of Solids and Structure*, 30(13),1737-44, 1993.

[6] Bert, C.W., Malik, M., Free vibration analysis of tapered rectangular plates by differential quadrature method: a semi- analytical approach, *Journal of Sound and Vibration,* 190(1), 41-63, 1996.

[7] Bert, C.W., Wang, Z., Striz, A.G., Convergence of the DQ method in the analysis of an isotropic plates, *Journal of Sound and Vibration*, 170(1), 140-44, 1994.

[8] Bert, C.W., Malik, M., Differential quadrature method in computational mechanics: a review, *Applied Mechanics Review*, 49(1), 1-28, 1996.

[9] Bert, C.W., Wang, Z., Striz, A.G., Static and free vibrational analysis of beams and plates by differential quadrature method, *Acta Mechanica,*102, 11-24, 1994.

[10] Björck, A., Pereyra, V., Solution of Vandermonde system of equations, *Mathematical computing,* 24, 893-903, 1970.

[11] Civalek, Ö., Finite Element analysis of plates and shells, *Elazığ: Fırat University (in Turkish),* 1998.

[12] Shu, C., Xue, H., Explicit computations of weighting coefficients in the harmonic differential quadrature, *Journal of Sound and Vibration*, 204(3), 549-55, 1997.

[13] Liew, K.M., Teo, T.M., Three dimensional vibration analysis of rectangular plates based on differential quadrature method, *Journal of Sound and Vibration,* 220(4), 577-99, 1999.

[14] Timoshenko, S.P., Gere, J.M., Theory Elastic Stability, McGraw-Hill, Second Edition, Tokyo, 1959.

[15] Chajes, A., Principles of Structural Stability Theory, Prentice-Hall, New Jersey, 1974.

[16] Wang, X., Striz, A.G., Bert, C.W., Buckling and vibration analysis of skew plates by the differential quadrature method, *AIAA Journal*, 32(4), 886-889, 1994.

[17] Wang, X., Bert, C.W., Striz, A.G., Differential quadrature analysis of deflection, buckling and free vibration of beams and rectangular plates, Computers and Structures, 48(3), 473-479, 1993.

[18] Wei, G.W., A new algorithm for solving some mechanical problems, *Comput. Methods Appl. Mech. Eng*., 190, 2017-2030, 2001.

[19] Wei, G.W., Vibration analysis by discrete singular convolution, *Journal of Sound and Vibration,* 244, 535-553, 2001.

[20] Wei, G.W., Discrete singular convolution for beam analysis, *Engineering Structures*, 23, 1045-1053, 2001.

[21] Akgöz, B., Civalek, O., Effects of thermal and shear deformation on vibration response of functionally graded thick composite microbeams, *Composites Part B: Engineering* 129, 77-87, 2017.

[22] Civalek, O., Geometrically non-linear static and dynamic analysis of plates and shells resting on elastic foundation by the method of polynomial differential quadrature (PDQ), Fırat University, Elazığ, 2004.

[23] Civalek, O., Demir, C., Buckling and bending analyses of cantilever carbon nanotubes using the euler-bernoulli beam theory based on non-local continuum model, *Asian Journal of Civil Engineering,* 12(5), 651-661, 2011.

[24] Akgoz, B., Civalek, O., Nonlinear vibration analysis of laminated plates resting on nonlinear two-parameters elastic foundations, *Steel and Composite Structures*, 11(5), 403-421, 2011.

[25] Civalek, O., Acar, M.H., Discrete singular convolution method for the analysis of Mindlin plates on elastic foundations, *International Journal of Pressure Vessels and Piping*, 84(9), 527-535, 2007.

[26] Civalek, O., Yavas, A., Large deflection static analysis of rectangular plates on two parameter elastic foundations, International journal of science and technology, 1(1), 43-50, 2006.

[27] Civalek, O., Kiracioglu, O., Free vibration analysis of Timoshenko beams by DSC method, *International Journal for Numerical Methods in Biomedical Engineering,* 26(12), 1890-1898, 2010.

[28] Demir, C., Civalek, O., A new nonlocal FEM via Hermitian cubic shape functions for thermal vibration of nano beams surrounded by an elastic matrix, *Composite Structures,* 168, 872-884, 2017.

[29] Mercan, K., Demir, C., Civalek, O., Vibration analysis of FG cylindrical shells with power-law index using discrete singular convolution technique, *Curved and Layered Structures,* 3(1), 82-90, 2016.

[30] Demir, C., Civalek, O., On the analysis of microbeams, *International Journal of Engineering Science*, 121, 14-33, 2017.

[31] Civalek, O., Geometrically nonlinear dynamic and static analysis of shallow spherical shell resting on two-parameters elastic foundations, *International Journal of Pressure Vessels and Piping*, 113, 1-9, 2014.